Analyst

ROYAL SOCIETY OF CHEMISTRY

MINIREVIEW

View Article Online
View Journal | View Issue

Cite this: *Analyst*, 2025, **150**, 2979

Biological functions and detection strategies of magnesium ions: from basic necessity to precise analysis

Tianwei Liu,†[a] Lan Wang,†[a] Siying Pei,[a] Shuo Yang,[a] Jiayi Wu,[a] Wei Liu*[b] and Qiong Wu *[a]

Magnesium is a ubiquitous element in the natural environment and plays an indispensable role in various biological processes in living organisms. This review focuses on the diverse functions of magnesium ions (Mg^{2+}) in living cells, particularly emphasizing their role in the immune and cardiovascular systems. We discuss how Mg^{2+} regulates key cellular processes, including enzyme catalysis, cellular signaling and nucleic acid structural stabilization, and explore the adverse effects of magnesium imbalance, which has been associated with numerous diseases ranging from cardiovascular to neurological disorders. Given these critical functions, accurate measurement of Mg^{2+} is essential. Thus, we also summarize a variety of analytical techniques for Mg^{2+}, ranging from traditional methods like atomic absorption spectrometry and electrochemical sensors to emerging approaches, such as fluorescent probe methods and X-ray fluorescence strategies. Bringing together recent advances in Mg^{2+} detection with a deeper understanding of its biological role, this review aims to promote the systematic integration of Mg^{2+} research in biomedical and clinical practice, in particular in the field of disease diagnosis and treatment.

Received 14th April 2025,
Accepted 14th June 2025

DOI: 10.1039/d5an00425j

rsc.li/analyst

1. Introduction

Magnesium is the fourth most abundant mineral in the human body, after calcium, sodium and potassium, and is involved in a wide range of physiological functions, including the regulation of potassium channels and the maintenance of bone health. The human body contains about 25 grams of magnesium, of which about 60% is stored in the bones, with the remainder distributed in the soft tissues and body fluids as free magnesium ions (Mg^{2+}).[1] The precise regulation of

[a]*State Key Laboratory of Flexible Electronics (LoFE) & Institute of Advanced Materials (IAM), School of Flexible Electronics (Future Technologies), Nanjing Tech University (Nanjing Tech), Nanjing 211816, China. E-mail: iamqwu@njtech.edu.cn*
[b]*School of Flexible Electronics (SoFE) & Henan Institute of Flexible Electronics (HIFE), Henan University, Zhengzhou 450046, China. E-mail: weiliu@henu.edu.cn*
† These authors contributed equally to this work.

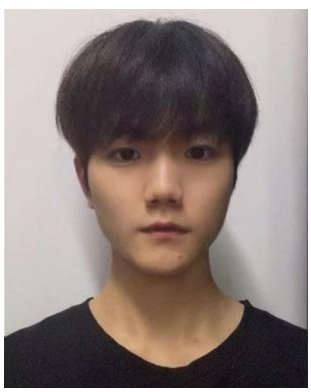

Tianwei Liu

Tianwei Liu received his BSc degree in applied chemistry from Chizhou college in 2022. He has been studying for a MS degree in Organic Chemistry since 2022 at the School of Flexible Electronics (Future technologies), Nanjing Tech University under the supervision of associate professor Qiong Wu. His research interest focuses on developing fluorescent probes for the detection of Mg^{2+}.

Lan Wang

Lan Wang received her BSc degree in Pharmacy from Wuhan University of Bioengineering in 2019. She is now a PhD candidate in School of Flexible Electronics (Future technologies), Nanjing Tech University (NanjingTech). Her current research interest is the design and application of mitochondria-targeted optical materials.

Mg^{2+} concentration is crucial for maintaining cellular function,[2] as it can participate in catalytic reactions as a cofactor for numerous key enzymes and is also involved in cellular signaling, gene expression regulation, and cell cycle control at multiple levels. Furthermore, Mg^{2+} plays a pivotal role in nerve conduction, muscle contraction, and cardiovascular function.[3] Its biological functions extend beyond the biochemical reactions in which it is directly involved. It also exerts indirect regulatory effects on a multitude of physiological processes by influencing intra- and extracellular ionic homeostasis.[4] For example, the synergy between Mg^{2+} and calcium ions (Ca^{2+}) is crucial for the proper functioning of the heart and muscles.

Although Mg^{2+} plays a critical role in biological activities, an imbalance in its levels—whether deficient or excessive—can lead to significant health problems. Mg^{2+} deficiency is a global public health challenge, with hypomagnesemia (Mg^{2+} concentrations below the normal range) being associated with a range of health problems, including high blood pressure, diabetes, metabolic syndrome, nerve damage, premature aging of cells, and the effects of chemotherapy on cancer. On the other hand, the relatively uncommon form of hypermagnesemia (abnormally elevated Mg^{2+} concentrations) is strongly associated with chronic kidney disease.[5] It is, therefore, of great importance to study the mechanisms regulating Mg^{2+} in cellular processes in order to gain a deeper understanding of these disorders and to develop more effective treatments.

Given the importance of Mg^{2+} in health and disease, accurate measurement of Mg^{2+} levels is essential, and a wide range of detection techniques have been developed. From the early days of simple colorimetric methods to today's chemical imaging techniques, each of these methods has its own strengths and weaknesses in terms of sensitivity, accuracy, and applicability, providing varying degrees of insight into understanding the dynamics of Mg^{2+} in living organisms.[6] However, due to the wide distribution of Mg^{2+} *in vivo* and the significant variability in its concentration, it may be difficult for routine assays to accurately reflect the state of Mg^{2+} at the cellular or tissue level, which poses a considerable challenge for accurate detection. In view of this, the creation of novel biomarkers and more accurate detection techniques has emerged as a prominent area of research in recent years. Fluorescence imaging has become a powerful and economical method for real-time tracking of Mg^{2+} distribution, absorption and movement due to its increased sensitivity, non-invasive nature, and superior spatial and temporal resolution.[7]

In this review, we provide a comprehensive overview of the physiological roles and detection methods of Mg^{2+}, with a special focus on the recent contributions of non-fluorescent and fluorescent probes to the detection of Mg^{2+}. These advances in technology will provide more accurate diagnostic tools for disease and increase our understanding of the potential role of Mg^{2+} in the prevention and treatment of disease. This review aims to assess the current technological limitations and explore the prospects for progress in this field.

2. Magnesium homeostasis in the human body

As the most abundant divalent cation in cells, Mg^{2+} plays an irreplaceable role in these human physiological functions, from regulating a wide range of immune cells to maintaining the structural stability of nucleic acids.[8] However, abnormal Mg^{2+} levels can trigger diseases such as high blood pressure and irregular heartbeat, so the body needs to keep Mg^{2+} levels in balance to stay healthy. Below, we will highlight the relationship between Mg^{2+} and various physiological systems.[9]

2.1 Immune function

Mg^{2+} is instrumental in modulating the immune system, specifically in the management of diverse immune cell functions.[10,11] For the innate immune system, Mg^{2+} deficiency activates polymorphonuclear leukocytes, leading to augmented phagocytosis and oxidative stress.[12] Conversely, in monocytes,

Wei Liu

Wei Liu received her PhD degree in Chemistry at Johannes Gutenberg University of Mainz (Germany) in 2024. She is currently working as an associate professor at Henan University and the Henan Institute of Flexible Electronics (HIFE). Her current research focuses on biomolecular detection and wearable electronic devices.

Qiong Wu

Qiong Wu received her PhD degree in Chemistry from Ewha Womans University in 2012. She got postdoctoral training in the same university and Nanjing Tech University under the supervision of Prof. Jinheung Kim and Academician Wei Huang. Then, she obtained an associate professor position at the School of Flexible Electronics (Future technologies) in 2018. Her research interests mainly focus on functional materials for biological application.

Mg^{2+} supplementation reduces cytokine production in response to toll-like receptor (TLR) stimulation.[13] Mg^{2+} is also essential in the modulation of the adaptive immune system, influencing the development, maturation and expansion of lymphocytes.[14] Moreover, recent structural biology studies have demonstrated that various ion channels and transporters associated with Mg^{2+} (such as MgtE, CorA, and CorC) maintain Mg^{2+} homeostasis in the immune system by precisely controlling Mg^{2+} transmembrane transport. These channel domains facilitate the movement of various cations, including Mg^{2+} and Ca^{2+}, across different subcellular compartments. It has been established that, among these, the TRPM7 protein is highly expressed in cells such as white blood cells and in various organs, including the heart and kidneys.[15,16] It has been demonstrated that TRPM7 plays a pivotal role in the activation, proliferation, and survival of T and B cells. For example, mice lacking TRPM7 exhibit substantial abnormalities in T cell development and B cell maturation. Nevertheless, this effect could be partially reversed by culturing cells in a medium enriched with high concentrations of Mg^{2+}.[17,18]

Notably, Mg^{2+} is critical for modulating the activity of $CD8^+$ T cell effector functions. $CD8^+$ T cells are an integral part of the adaptive immune system and play a key role in identifying and eliminating infected or malignant cells. In mice, a reduction in serum Mg^{2+} concentration has been observed to impair $CD8^+$ T-cell responses to influenza A virus, diminish T-cell activation, and exacerbate pathology.[18] As posited by Lötscher *et al.*, Mg^{2+} influences the effector function of $CD8^+$ T cells by mediating LFA-1 (leukocyte function-associated antigen 1) receptor sensing.[19] LFA-1 is an important co-stimulatory molecule, and Mg^{2+} is able to promote conformational changes of LFA-1 and enhance $CD8^+$ T cell activation, metabolic reprogramming, immune synapse formation, and other key processes. These processes are crucial in anti-tumour immunity. Mg^{2+} enhances the anti-tumour effect of CAR-T cells in the treatment of large B-cell lymphoma and non-small cell lung cancer through its regulatory effect on LFA-1. Research findings have indicated that patients with elevated serum Mg^{2+} levels show a higher chance of survival after treatment with CAR-T cell therapy and immune checkpoint inhibitors (Fig. 1).

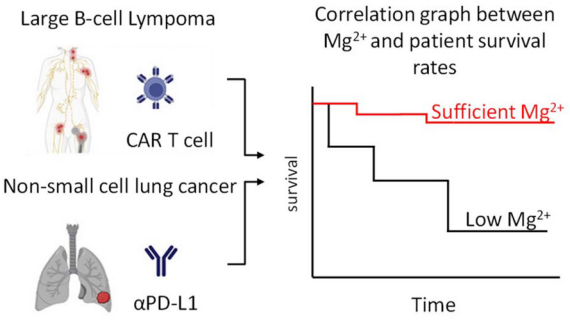

Fig. 1 CAR T-cell therapy and immune checkpoint inhibition in the treatment of large B-cell lymphoma and non-small cell lung cancer and the impact of Mg^{2+} levels on patient survival. Adapted with permission from ref. 19, Copyright 2022, Elsevier.

Inflammation constitutes a prevalent form of immune system response, serving a protective function against infection and injury. Studies have shown that Mg^{2+} transporter proteins (*e.g.*, TRPM7 and MagT1) are involved in the regulation of inflammation. For example, Rios *et al.* observed the development of cardiac hypertrophy, inflammation and fibrosis in TRPM7 heterozygous mice, accompanied by decreased levels of Mg^{2+}, upregulated expression of inflammatory factors and transcription factors, and increased macrophages.[20] In contrast, Schilling *et al.* found that inhibition of TRPM7 resulted in the abrogation of IL-4-induced macrophage proliferation and the prevention of polarization to an anti-inflammatory M2 phenotype.[21] Furthermore, Li *et al.* demonstrated that endocytosis of Mg^{2+} can be modulated by regulating MagT1 function, which affects T-cell signaling and activation. Loss of function of the MagT1 gene results in an immunodeficiency syndrome known as XMEN (X-linked immunodeficiency with magnesium deficiency, EBV infection and neoplasia).[22,23]

2.2 Cardiovascular system

Mg^{2+} plays a key role in maintaining cardiovascular health in humans. Firstly, Mg^{2+} stabilizes myocardial excitability and contractility by acting on calcium channels and sodium–potassium pumps. Secondly, Mg^{2+} regulates myocardial contractility by antagonizing Ca^{2+} movement within cardiomyocytes, and finally, Mg^{2+} exerts an anti-inflammatory effect, reduces vascular endothelial damage, promotes nitric oxide production and vasodilates blood vessels (Fig. 2).[24,25]

Mg^{2+} has been demonstrated to be intimately associated with the precise regulation of electrophysiological activities of cardiomyocytes. The central mechanism of action of Mg^{2+} is reflected in the dynamic processes of cardiac action potential. The myocardial action potential cycle is generally divided into five phases, in which Mg^{2+} acts mainly in the second and third phases. During the second phase of the cardiac action potential, Mg^{2+} plays a regulatory role in the inward flow of Ca^{2+}, preventing Ca^{2+} overload by inhibiting L-type Ca^{2+} channels.[26,27] Mg^{2+} binds to Ca^{2+} channels, affecting Ca^{2+} flow, and its effect on Ca^{2+} channel current may be influenced by the phosphorylation state of the channel.[28] In the third phase, delayed collation of potassium channels drives cellular repolarization *via* fast-activating (I_{kr}) and slow-activating (I_{ks}) currents, and Mg^{2+} specifically regulates this process: high concentrations of Mg^{2+} selectively inhibit the I_{ks} current in cardiomyocytes, thereby delaying the transition from plateau phase to repolarization.[29,30] In addition, Mg^{2+} also significantly affects the third and fourth phases of the action potential by reducing K^+ efflux at the end of repolarization.[31]

There has been a recent surge of interest in the role of Mg^{2+} in cardiac excitation–contraction coupling, with a particular focus on its impact on Ca^{2+} mobilization.[32] Mg^{2+} interacts with a variety of proteins and plays a key role in the regulation of intracellular Ca^{2+} concentrations. Mg^{2+} is also an essential component of adenosine triphosphate (ATP) that binds to the cardiac Ca^{2+} ATPase and regulates the sodium–calcium exchanger NCX1's affinity for Ca^{2+}.[33,34]

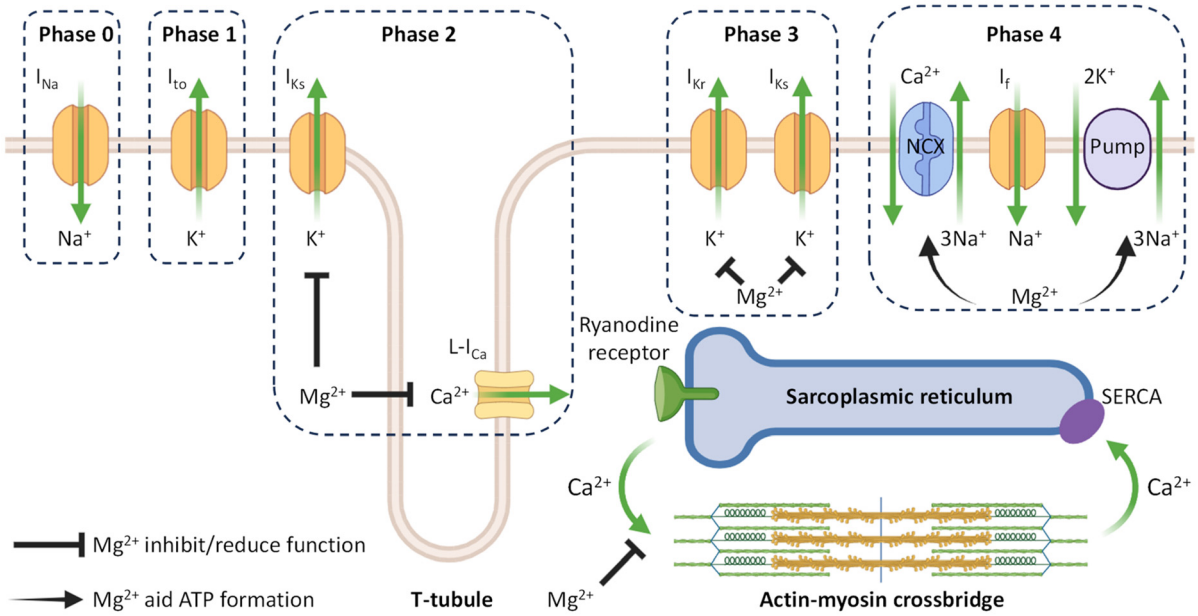

Fig. 2 The role of Mg^{2+} in the excitation-contraction coupling of cardiomyocytes. The mycardial action potential cycle consists of five phases. Phase 0: rapid depolarisation; Phase 1: initial repolarisation; Phase 2: plateau phase; Phase 3: repolarisation; Phase 4: resting phase. ATP: adenosine triphosphate; Ca^{2+}: calcium ions; I_{Na}: voltage-dependent sodium channel; I_{to}: transient outward potassium channel; I_{ks}: slow component of delayed rectifier potassium channel; I_{kr}: rapid component of delayed rectifier potassium channel; L-I_{ca}: L-type calcium channel; I_f: "funny" pacemaker current; K^+: potassium ions; Na^+: sodium ions; Mg^{2+}: magnesium ions; NCX: sodium–calcium exchanger; SERCA: sarcoplasmic/endoplasmic reticulum calcium ATPase. Adapted with permission from ref. 24, Copyright 2018, Elsevier.

The significant vasodilatory effect of Mg^{2+} is achieved through a multitude of mechanisms. Lack of Mg^{2+} increases oxidative stress and endothelial cell injury, leading to an elevation in reactive oxygen species (ROS) and inflammation, which weakens endothelial function and affects vasodilatory capacity. Meanwhile, moderate amounts of Mg^{2+} can upregulate the expression and activity of endothelial-type nitric oxide synthase (eNOS), which significantly increases the synthesis and release of nitric oxide (NO) and decreases the synthesis of the vasoconstrictor factor endothelin-1, ultimately facilitating vasorelaxation and lowering blood pressure.[35,36] Furthermore, Mg^{2+} has been shown to affect vascular function by regulating Ca^{2+} influx into vascular smooth muscle cells. Reducing Ca^{2+} influx results in a decrease in vasoconstriction and an increase in vasodilation.[37]

2.3 Skeletal and muscular

As a key regulator of bone metabolism, Mg^{2+} maintains the dynamic homeostasis and structural integrity of bone tissue through a multi-dimensional mechanism. Human bone is a major storage site for Mg^{2+}, and Mg^{2+} interacts with hydroxyapatite crystals in bone to increase the solubility of Ca^{2+} and phosphate, affecting crystal growth and size. Mg^{2+} also promotes osteoclast proliferation, and its deficiency leads to reduced bone formation, such as reduced osteoblast number and bone mass in magnesium-deficient rats.[38]

Mg^{2+} is essential for Ca^{2+} metabolism. As well as assisting in absorbing Ca^{2+}, Mg^{2+} helps to maintain Ca^{2+} balance by modulating the secretion of parathyroid hormone (PTH) and the function of vitamin D. PTH is released by the parathyroid glands when there is a detected drop in blood Ca^{2+} levels. Abnormalities in PTH levels, whether too high or too low, can lead to disturbances in Ca^{2+} metabolism and bone disorders, which can result in conditions such as osteoporosis or bone softening.[39] In addition, Mg^{2+} is an essential cofactor for many of the enzymes involved in the metabolism and regulation of vitamin D. The conversion of vitamin D to its active form, 1,25(OH)2D3, occurs in two steps. Initially, vitamin D3 is converted to 25(OH)D in the liver by magnesium-dependent 25-hydroxylase, and then to its active form, 1,25(OH)2D, by 1α-hydroxylase in the kidneys. Mg^{2+} is also required for the activity of vitamin D-binding protein (DBP), which is responsible for transporting vitamin D in the blood. While 1,25(OH)2D3 synthesis also occurs in other tissues, such as the brain and testes, the majority of serum 1,25(OH)2D3 is produced in the kidneys (Fig. 3).[40] The steroid hormone 1,25-dihydroxyvitamin D3 (1,25(OH)2D3) stimulates the vitamin D receptor and, consequently, the transcription of genes that are sensitive to vitamin D signaling.[41] While vitamin D enhances intestinal Mg^{2+} absorption, a deficiency in Mg^{2+}, which is associated with vitamin D-dependent rickets, results in a reduction in 1,25(OH)2D3 levels.[42] The whole process reflects the bidirectional regulatory role of Mg^{2+} in vitamin D metabolism homeostasis.

This calcium–magnesium–vitamin D triangular regulatory network plays a pivotal role in maintaining the homeostasis of

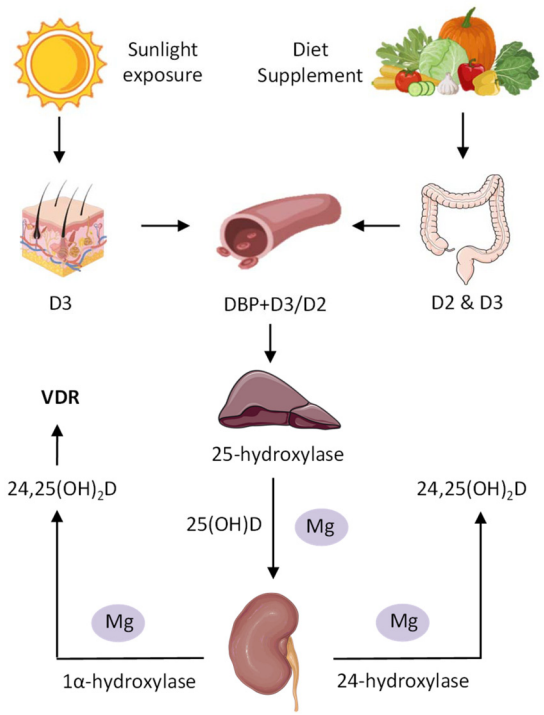

Fig. 3 Mg^{2+} is essential for the activity of vitamin D-binding protein (DBP), which is responsible for transporting vitamin D (*e.g.*, D2 and D3) in the blood. [VDR: vitamin D receptors]. Adapted with permission from ref. 40, Copyright 2019, Elsevier.

the skeletal system, with its effects extending to the level of skeletal muscle function. It affects muscle contraction by competing with Ca^{2+} for binding sites on troponin C and myosin.[43] In the resting state, because the concentration of Mg^{2+} in muscle cells is much higher than that of Ca^{2+}, Mg^{2+} occupies the Ca^{2+} binding sites and prevents muscle contraction. Upon the release of Ca^{2+} from the sarcoplasmic reticulum, Ca^{2+} displaces Mg^{2+}, triggering muscle contraction; in cases of Mg^{2+} deficiency, even a small amount of Ca^{2+} can displace Mg^{2+}, leading to excessive muscle contraction, which can cause muscle spasms and twitching. Therefore, Mg^{2+} is important for maintaining normal muscle activity and preventing involuntary contractions.

2.4 Energy metabolism

ATP is the primary energy currency of the cell. Mg^{2+} is essential for intracellular ATP synthesis. Due to the ability of Mg^{2+} to bind with inorganic phosphate, ATP, phosphocreatine, and other phosphorus metabolisms to form complexes, it can have a significant impact on numerous metabolic reactions, particularly those related to carbohydrate metabolism and cellular bioenergetics, which release energy through hydrolysis of the phosphate group. In addition, Mg^{2+} plays a crucial role in maintaining the ATP structure, thereby enhancing energy transfer efficiency.[44] Glycolysis represents a fundamental aspect of cellular metabolism, whereby glucose is broken down into pyruvate, releasing energy for cellular activity. Mg^{2+} serves as an indispensable cofactor for numerous glycolytic enzymes during glycolysis. By stabilizing the negatively charged ATP, Mg^{2+} facilitates the recognition of ATP by glycolytic enzymes, including hexokinase, phosphofructokinase, phosphoglycerate kinase and pyruvate kinase, thereby enabling the smooth progression of the reaction. In addition, aldolase and enolase require Mg^{2+} to maintain enzyme stability and activity, although they do not directly depend on the binding between Mg^{2+} and ATP.[45] A lack of Mg^{2+} within a cellular milieu can lead to a decrease in the efficacy of glycolysis, affecting energy supply. This phenomenon is particularly evident in cells with high metabolic demands, such as muscle or brain cells, and may result in fatigue or metabolic disorders.

Mitochondrial function is a key aspect of energy metabolism, and its efficient operation directly determines the level of cellular energy supply. Mg^{2+}, as a key regulator in this process, plays an irreplaceable role in maintaining the activity of three key mitochondrial dehydrogenases, including dehydrogenase (IDH), α-ketoglutarate dehydrogenase complex (OGDH), and pyruvate dehydrogenase (PDH) (Fig. 4).[46] IDH is directly stimulated by the Mg^{2+}-isocitrate complex, while OGDH is activated by free Mg^{2+}. In addition, Mg^{2+} promotes the activation of the PDH through indirect action on pyruvate dehydrogenase phosphatase. This phosphatase activates pyruvate decarboxylase (a key component of PDH) by removing the phosphate group from the enzyme. In addition, Mg^{2+} is a key activator of ATP production by the mitochondrial Fo/F1-ATPase complex, thereby significantly affecting ATP synthesis, mitochondrial membrane potential, and cellular respiration processes.[47] In addition to Mg^{2+}, iron (Fe) within heme and iron–sulfur clusters in the electron transport chain are vital for mitochondrial oxidative phosphorylation, and copper ion (Cu^{2+}) serves as a cofactor in cytochrome coxidase.[48,49] In the

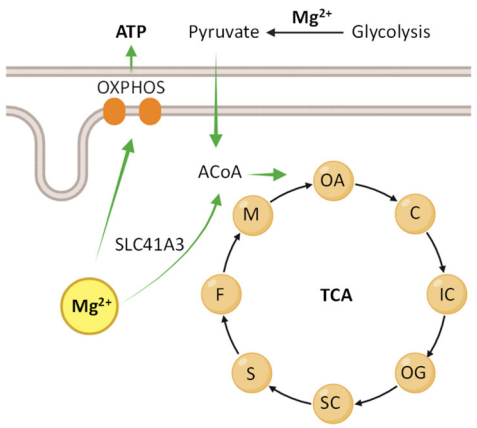

Fig. 4 Regulation of mitochondrial functions by Mg^{2+}. TCA: tricarboxylic acid cycle/Krebs cycle; ACoA: acetyl coenzyme A; C: citrate; IC: isocitrate; OG: 2-oxoglutarate; SC: succinyl coenzyme A; S: succinate; F: fumarate; M: malate; OA: oxaloacetate; SLC41A3: mitochondrial Mg^{2+} efflux system; OXPHOS: oxidative phosphorylation. Adapted with permission from ref. 46. Copyright 2017, Wiley.

case of α-ketoglutarate as an oxidizing substrate, OGDH represents the primary step in oxidative phosphorylation, which is regulated by Mg^{2+}. Conversely, in the case of succinate as a substrate, ATP synthase exhibits Mg^{2+} sensitivity.[50] The intracellular Mg^{2+} dynamic equilibrium is maintained through interactions with ATP, the source of energy. Mg^{2+} levels are lower in the brains of patients with mitochondrial cytoskeletal disorders. Coenzyme Q10 supplementation enhances mitochondrial function and oxidative phosphorylation, indirectly promoting mitochondrial Mg^{2+} uptake and increasing cytoplasmic Mg^{2+} levels.[51]

2.5 Nervous function

In the brain, Mg^{2+} is not only involved as a metabolite in all biochemical pathways, but also plays a fundamental role in neural signaling and the maintenance of ionic homeostasis, and has been implicated in a variety of neurological disorders. Mg^{2+} inhibits the inward flow of Ca^{2+} by blocking voltage-dependent channels and also prevents calcium release mediated by inositol 1,4,5-trisphosphate and ryanodine receptors. The inhibitory effect of Mg^{2+} helps to avoid excess Ca^{2+} influx, thereby preventing neuronal hyperexcitability or neurotoxicity.[52]

The importance of Mg^{2+} is further demonstrated by its association with *N*-methyl-D-aspartate (NMDA) receptors. Glutamate, as the predominant excitatory neurotransmitter in the central nervous system (CNS), plays a key role in neuronal communication. Glutamate facilitates the influx of Ca^{2+}/sodium ions (Na^{+}) and the efflux of potassium ions (K^{+}) when it is bound to NMDA receptors (Fig. 5).[53] It has been shown in the presence of elevated membrane potentials and low Mg^{2+} levels, activation of NMDA receptors is increased and closure of NMDA channel is decreased, which in turn results in neuronal hyperexcitability, oxidative stress, and cell death. In addition, Mg^{2+} is involved in regulating the inhibitory effects of gamma-aminobutyric acid (GABA) receptors and influences the inward flux of chloride ions (Cl^{-}), which contributes to hyperpolarization of nerve cells and inhibit neuronal excitability.[54] Additionally, Mg^{2+} is crucial for the maintenance of the blood–brain barrier's (BBB) structural and functional integrity. This is achieved through the modulation of Ca^{2+} concentrations in endothelial cells, regulating tight junction proteins.[55] Alongside Mg^{2+}, Ca^{2+} acts as a key second messenger in neuronal signaling, mediating neurotransmitter release and synaptic plasticity, while zinc (Zn^{2+}) concentrated in synaptic vesicles modulates neurotransmission, particularly at glutamatergic synapses.[56] By modulating neuronal excitability, reducing neuroinflammation and improving neurotransmitter homeostasis, Mg^{2+} can help prevent and treat a wide range of neurological disorders. Numerous studies have shown that Mg^{2+} deficiency is strongly associated with a variety of neurological disorders, including Alzheimer's disease, Parkinson's disease, and stroke.[57] Adding Mg^{2+} to the diet can be effective in reducing symptoms and slowing the progression of these conditions.

2.6 Nucleic acids

Mg^{2+} acts as a critical structural stabilizer for nucleic acids (DNA and RNA), orchestrating their three-dimensional (3D) architecture through charge neutralization and coordination chemistry. Firstly, Mg^{2+} is capable of forming stable complexes with the phosphate groups of DNA, which helps to stabilize

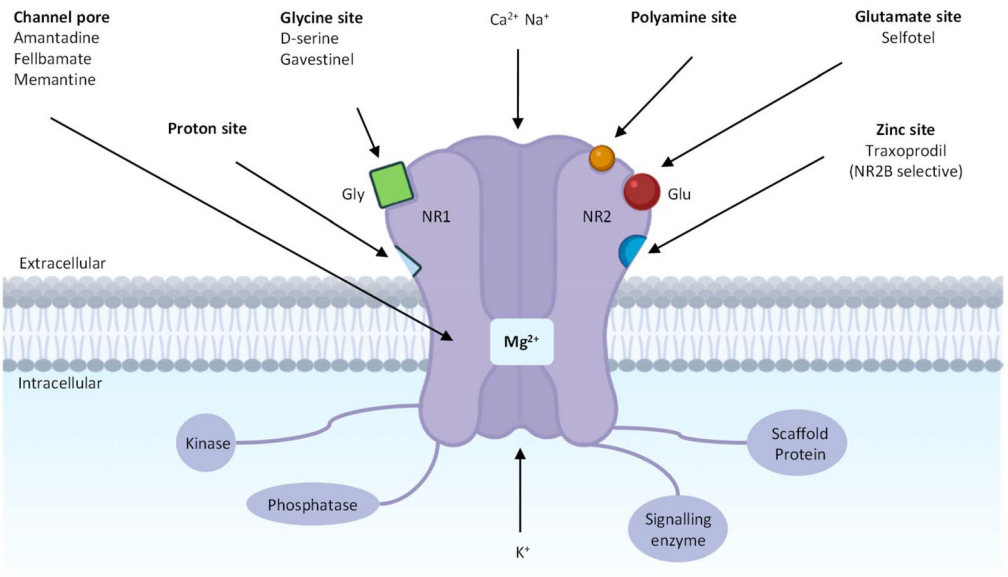

Fig. 5 Glutamatergic *N*-methyl-D-aspartate receptor with magnesium-mediated block of calcium channel. In the state of neuronal inactivity, Mg^{2+} exerts an inhibitory effect on the NMDA receptor channels, thereby impeding the influx of Ca^{2+}/Na^{+} into the cell, thus preventing excessive neuronal excitation. Conversely, when the neuron becomes active and depolarises, Mg^{2+} leaves the channel, allowing Ca^{2+}/Na^{+} to pass through. Adapted with permission from ref. 53, Copyright 2008, Elsevier.

the double helix structure of DNA. The positive charge of Mg^{2+} is attracted to the negative charge on the DNA backbone, thereby reducing the repulsive forces between the strands of DNA.[58] However, at very low or very high concentrations, Mg^{2+} can destabilize DNA by affecting its structure, enzyme activity and repair mechanisms.[59] Secondly, Mg^{2+} forms ligands with phosphate groups and oxygen atoms of nucleotides, thereby further stabilizing the nucleic acid structure. In particular, Mg^{2+} contributes to the formation of complex secondary and tertiary structures in RNA, including the folding of transfer RNA (tRNA) and ribosomal RNA (rRNA) (Fig. 6).[60] Mg^{2+} is also involved in the stabilization of superhelices, preventing DNA and RNA from unraveling or denaturing at high temperatures or under other adverse conditions. Therefore, Mg^{2+} plays a pivotal role in maintaining the functional and structural integrity of nucleic acids.[61,62]

Additionally, Mg^{2+} serves as a cofactor for numerous enzymes involved in DNA and RNA metabolism. Firstly, Mg^{2+} acts as an enzyme cofactor, assisting enzymes such as DNA polymerase and RNA polymerase in stabilizing their active sites and catalyzing the formation and breaking of phosphodiester bonds. By forming a complex with substrates such as nucleotides, Mg^{2+} reduces the activation energy of the reaction and facilitates the binding of the substrate to the enzyme. In addition, Mg^{2+} helps to maintain the correct 3D conformation of enzymes, a factor that is critical for their peak enzymatic activity. The two Mg^{2+} ions in the bimetallic mechanism function in concert to catalyze reactions and enhance their efficiency. Alterations in Mg^{2+} concentration also regulate enzyme activity, influencing DNA replication, repair, and other crucial processes.[63]

Nucleic acid synthesis is the process of DNA replication and RNA transcription that involves the polymerization of nucleotides. Mg^{2+} plays a pivotal role in both processes, assisting in the incorporation of nucleotides and facilitating the formation of phosphodiester bonds, thereby ensuring the precision and efficiency of nucleic acid synthesis.[64,65] Mg^{2+} stabilizes the nucleic acid structure by neutralizing the negative charge of the DNA/RNA, thus facilitating the chemical reaction. Mg^{2+} also promotes the hydrolysis of nucleoside triphosphates (NTP) by neutralizing its negative charge, thereby providing the energy necessary for nucleic acid synthesis.[66] These actions ensure the stability and function of nucleic acids, which are essential for normal physiological cell function and the regulation of gene expression.

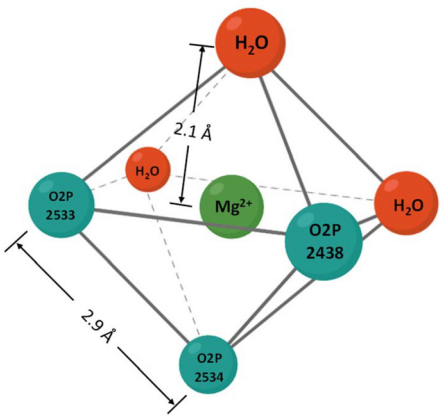

Fig. 6 Structure of the Mg^{2+}/RNA chelate (Mg^{2+} 8001 from 23S rRNA of the Haloarcula LSU; PDB entry 1JJ2). Adapted with permission from ref. 60, Copyright 2012, Elsevier.

3. The detection strategies of Mg^{2+}

In recent years, the detection strategy of Mg^{2+} has become a significant field in environmental monitoring, food safety and medical diagnosis. At present, the prevalent detection methods can be categorized into two types: non-fluorescent probe detection and fluorescent probe detection. Each detection method possesses distinct advantages and disadvantages in terms of sensitivity and selectivity, so the most suitable method needs to be selected based on the specific application scenario and requirements. The following section will outline the methods for detecting Mg^{2+} and their respective characteristics.[67,68]

3.1 Non-fluorescent probes detection of Mg^{2+}

Currently, a variety of non-fluorescent probe methods have been used for the qualitative and quantitative detection of Mg^{2+}, including atomic absorption spectrometry, electrochemical analysis, colorimetric/enzymatic methods, X-ray fluorescence spectrometry and nuclear magnetic resonance spectroscopy (Fig. 7). Each of these methods has its own advantages and provides different options for the detection of Mg^{2+}. Therefore, this section will focus on the non-fluorescent probe detection methods and discuss their specific applications in Mg^{2+} detection in detail.

3.1.1 Atomic spectrometry analysis. Atomic absorption spectrometry (AAS) is the oldest and most widely used technique for assessing Mg^{2+} in biological samples. It was first introduced by A. Walsh in the mid-20th century and is based on the principle that Mg^{2+} absorbs light at specific wavelengths.[69] AAS provides a sensitive and specific method for the identification of trace elements, which is easy to perform and economical, with the important advantage of being applicable to all biological samples.[70,71] However, there are some inherent limitations to the technique, including the need for sample preparation (usually in the form of acidic extracts) and the need for instrument calibration. Inductively coupled plasma-atomic emission spectrometry (ICP-AES) is a technique that has been proven to achieve detection through the emission of characteristic spectra after Mg^{2+} excitation.[72] It has significant advantages over AAS, such as the ability to detect multiple elements simultaneously, a wide linear range and high sensitivity analysis, and is particularly suitable for the determination of trace elements.[73,74] The selection of analytical methodology should be guided by the specific analytical require-

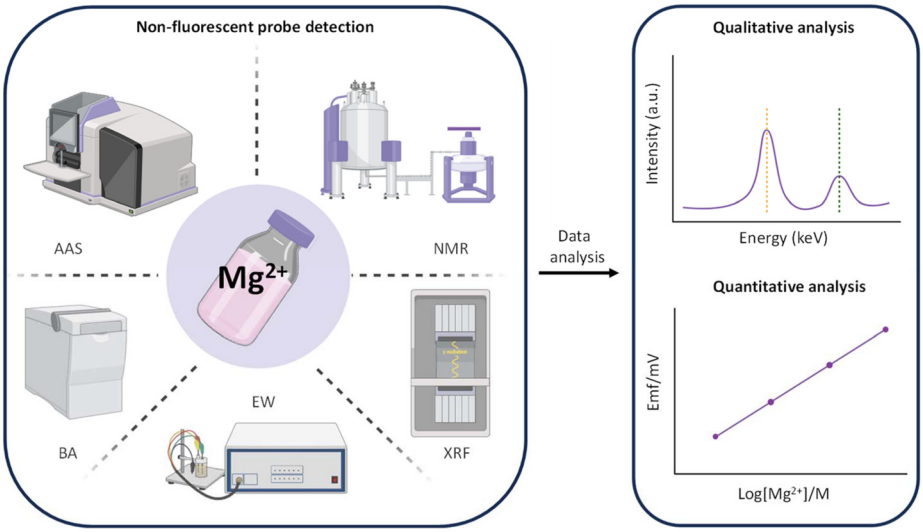

Fig. 7 Common non-fluorescent diagnostic assays for Mg^{2+}. AAS: atomic absorption spectrometer; NMR: nuclear magnetic resonance spectrometer; BA: biochemical analyser; EW: electrochemical workstation; XRF: X-ray fluorescence spectrometer.

ments, sample characteristics, cost-effectiveness, and laboratory capabilities.

3.1.2 Electrochemical analysis. The increasing use of electrochemical analysis in biochemical analysis covers many types of electrochemical sensors. Common electrochemical sensors can be categorized into different types, such as amperometric, potentiometric, voltammetric, impedimetric, photoelectrochemical and electrochemiluminescent sensors.[75] Electrochemical sensors for detection typically employ selective electrodes (ISEs) for potentiometric determination. These electrodes, in conjunction with a reference electrode, constitute an electrochemical system that detects the concentration of Mg^{2+} by measuring the alteration in electrode potential.[76,77] For example, Farahani *et al.* developed a novel 3D-printed Mg^{2+} potentiometric sensor for bioanalysis in microfluidic devices.[78] The sensor was fabricated using 3D printing technology by immobilizing a functionalized light-cured methacrylate-based ion-selective membrane (ISEM) on a carbon mesh/epoxy solid contact sensor (Fig. 8a). The 3D-printed Mg^{2+} selective electrode (3Dp-Mg^{2+}-ISE) exhibited an energetic response of 27.5 mV per decade with a linear range from 39 μM to 10 nM, covering physiologically and clinically relevant levels of Mg^{2+} in biofluids (Fig. 8b). The sensor also measures Mg^{2+} selectively, avoiding interference from other potentially common ions (Fig. 8c). Compared to polyvinyl chloride (PVC)-Mg^{2+}-ISE, 3Dp-Mg^{2+}-ISE has several advantages, particularly in terms of stability, resistance to biological contamination and large-scale production (Fig. 8d). The study also demonstrated the rapid prototyping and optimization capabilities of 3D printing technology for ISE fabrication, providing new opportunities for the development of next-generation field diagnostic devices. In their review published in 2018, Lvova *et al.* discussed the development of sensors with high selectivity and sensitivity through the use of specific ionic carriers and polymeric matrices, such as PVC, polypyrrole (PPy), poly(3,4-ethylenedioxythiophene) (PEDOT), *etc.*[79] The great value of electrochemical analysis in practical applications provides new insights and potential for the detection of Mg^{2+}. It is anticipated that this method will replace traditional analytical techniques, including AAS and ICP-AES, as a more efficient and rapid detection approach.

3.1.3 Colorimetric/enzymatic assays. Colorimetric techniques are widely utilized in clinical laboratories for the measurement of Mg^{2+} concentrations. The method is based on the use of specific metal complexing dyes that undergo a color change when bound to metal ions, thereby enabling quantitative analysis by spectrophotometry.[80,81] Four popular indicators currently in use include dimethylaniline blue (Magon),[82] methylnitrotoluene blue,[83] methyleneimine dyes,[84] and calmagite.[85] Although these indicators can be complex with Mg^{2+} and undergo a color change, their performance can be affected by interference from other cations. For example, Ca^{2+} exhibits a higher binding affinity for certain dyes (*e.g.*, Calmagite) than Mg^{2+}. This results in Ca^{2+} occupying the complexation sites preferentially, consequently leading to low Mg^{2+} measurements. Unlike the colorimetric method, enzymatic analysis relies on the physiological function of Mg^{2+} as a cofactor in numerous enzymatic reactions for the measurement process. It also relies on spectrophotometric analysis, but has the advantage over colorimetric methods in terms of improved selectivity for Mg^{2+} relative to other cations. To illustrate, the glucose-6-phosphate dehydrogenase (G6PD) method quantifies Mg^{2+} by measuring NADPH production, demonstrating no interference from Ca^{2+} and phosphate, although it may be influenced by lipemia.[86] Furthermore, the glycerol kinase method offers a rapid, straightforward and automated alternative for the quantification of Mg^{2+} by measuring the absorbance of a red product produced by activated glucokinase.[87] In

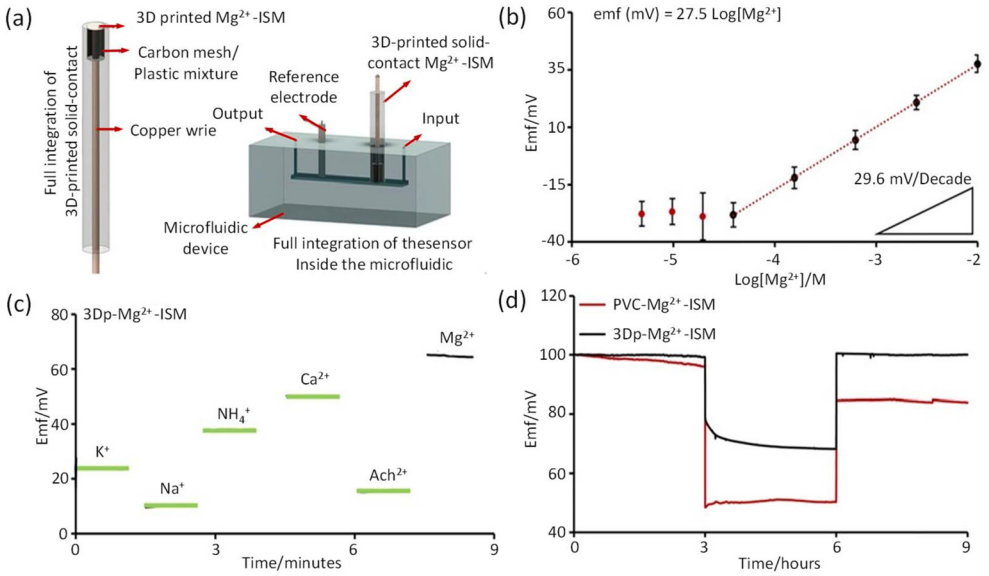

Fig. 8 Design, response characterization and application of 3D printed Mg^{2+} selective electrodes (3Dp-Mg^{2+}-ISE). (a) Schematic representation of 3Dp-Mg^{2+}-ISE integrated into the microfluidic device. (b) The linear response of the 3Dp-Mg^{2+}-ISE to Mg^{2+} is observed within a concentration range of 39 μM to 10 mM, showing a slope of 27.5 mV per decade (illustrated error bars are the standard deviation obtained from three separate Mg^{2+}-ISEs; inset triangle depicts a slope of 29.6 mV per decade). (c) Selectivity analysis of 3Dp-Mg^{2+}-ISE for different ions (1 mM). (d) The normalized results of the water layer test for PVC-Mg^{2+}-ISE and 3Dp-Mg^{2+}-ISE after being immersed in 1 mM Mg^{2+} solution for 3 hours, then in 1 mM KCl solution for 3 hours, and finally back in 1 mM Mg^{2+} solution for another 3 hours. Reproduced with permission from ref. 78, Copyright 2023, Royal Society of Chemistry.

general, the colorimetric assay is well-suited to rapid, low-cost experiments, whereas the enzymatic method is more appropriate for studies that require high accuracy and selectivity, as well as for more complex studies and analyses.

3.1.4 X-ray fluorescence (XRF). The detection of metallic elements has been a primary focus of chemical imaging research. The main methods used to visualize metallic elements in biological samples are based on X-ray emission spectroscopy techniques, including particle-induced X-ray emission (PIXE) and synchrotron X-ray fluorescence (SXRF).[88,89] XRF microscopy is particularly effective in this regard, as it excites the electrons of an atom's nucleus to produce characteristic X-rays, thereby enabling the detection of elements in samples. The initial proposal of utilizing X-rays for the detection of Mg^{2+} was put forth by Haigney *et al.* in 1995, marking the advent of X-ray applications in biological contexts.[90] Individual cells are analyzed by energy dispersive X-rays to measure the Mg^{2+} content of individual cells.[91] Furthermore, analytical scanning electron microscopy (ASEM) coupled with energy dispersive X-ray spectroscopy (EDS) has been demonstrated in clinical studies to be an effective method for monitoring Mg^{2+} and K^+ levels in diabetic patients, receiving Mg^{2+} supplementation therapy. This approach allows for the simultaneous detection of Mg^{2+} and other trace elements, which is advantageous in clinical settings.[92] These techniques offer novel insights into the intracellular function of Mg^{2+} and its potential role in diseases.

3.1.5 Nuclear magnetic resonance (NMR). NMR is a powerful analytical technique typically used to study molecular structure, dynamics, and chemical environments. NMR is most commonly used on atoms containing a specific nuclear spin (*e.g.*, ^1H, ^{13}C, and ^{15}N, *etc.*). While naturally occurring Mg^{2+} does not have a half spin, NMR can be used indirectly for detecting and studying Mg^{2+}, especially when Mg^{2+} interacts with organic molecules or ligands. For example, McFadden *et al.* employed β-radiation-detection nuclear magnetic resonance (β-NMR) spectroscopy to investigate the formation of complexes between Mg^{2+} and ATP in 1-ethyl-3-methylimidazole acetate (EMIM-Ac) solution.[93] Utilizing β-NMR spectroscopy, the researchers were able to observe the chemical shifts of these complexes and compare them with the results of quantum chemical calculations, thereby providing substantial experimental evidence for the structural and dynamic behavior of the complexes formed by Mg^{2+} and ATP in EMIM-Ac solution. However, NMR technology is still subject to restrictions on its clinical applications, mainly due to its limited flux and high costs associated with hardware and consumables, coupled with the need for specialized technical expertise to acquire and interpret NMR spectra. Nevertheless, NMR remains a valuable experimental tool in the field of elemental detection, offering a crucial means of elucidating cellular processes and biomolecule behaviors.

3.2 Fluorescent probes detection of Mg^{2+}

In recent years, fluorescence imaging has been increasingly applied to the study of Mg^{2+} because of its significant advantages in determining the dynamic behaviors of individual cells and observing them in real time. In order to better study the

amount of Mg^{2+} in cells or body fluids and to assess the mobility of this ion in the intra- and extracellular environment as well as between intracellular levels, a number of novel fluorescent probes have been developed for the detection of Mg^{2+}.[94] Therefore, recent advances in Mg^{2+} fluorescent probes based on common binding sites for Mg^{2+} will be discussed in this section.

3.2.1 Fluorescent probes for Mg^{2+} based on *o*-aminophenol-*N*,*N*,*O*-triacetic acid (APTRA) binding sites. Over time, the development of methods for the selective detection of Mg^{2+} has progressed at a gradual pace. In 1957, Hasselbach published his work, emphasizing the significance of Mg^{2+} in cellular processes.[95] However, over the past five decades, Ca^{2+} has been regarded as a crucial second messenger in rapid intracellular responses. As a result, many specialized fluorescent probes have been developed for the precise monitoring of Ca^{2+} levels in living cells, leading to a relative delay in the development of specific fluorescent probes for Mg^{2+}. In 2010, Trapani *et al.* referred to Mg^{2+} as the "forgotten cation", and Mg^{2+} probes have been progressively developed based on existing Ca^{2+} probes.[96] With the increasing research on Mg^{2+}, Mag-fura-2 was introduced as the first fluorescent Mg^{2+} indicator that achieves specific binding of Mg^{2+} based on *o*-aminophenol-*N*,*N*,*O*-triacetic acid (APTRA) motifs, allowing real-time monitoring of Mg^{2+} concentration in living cells.[97] A variety of fluorescent probes have been developed based on the APTRA binding sites, including Mag-Indo-1, Mag-Fura-4, Magnesium-Green, *etc*.[94] These probes provide a powerful tool for studying the role of Mg^{2+} in biological systems.

In a study inspired by the "fura" fluorophore, Buccella *et al.* successfully developed two Mg^{2+} red-shifted ratiometric fluorescent indicators, Mag–S and Mag–Se, by introducing sulfur or selenium into the azole group of the "fura" fluorophore.[98] It provides longer excitation and emission wavelengths and greater spacing between excitation bands, which is valuable for imaging intracellular Mg^{2+} ratiometric measurements. The red shifts exhibited by Mag–S and Mag–Se are more significant than those observed in Mag-Fura-2. The development of fluorescent probe technology has highlighted the constraints of utilizing fluorescence imaging in cellular and organismal contexts. BODIPY fluorophores are a preferred option for fluorescence imaging due to their high quantum yield and low cytotoxicity.[99] To this end, Lin *et al.* have developed two fluorescent probes capable of absorbing and emitting light in the visible spectrum when they bind to Mg^{2+} in aqueous solutions, leading to a significant increase in fluorescence intensity.[100] MagB1 and MagB2 are two fluorescence probes based on APTRA recognition motifs and different BODIPY fluorophores. MagB2, a red-emitting styrene BODIPY fluorescent probe, exhibits better metal selectivity and optical properties compared to green-emitting MagB1. MagB2 has a 58-fold fluorescence enhancement effect for Mg^{2+} detection and its Mg^{2+} dissociation constantly matches physiological concentrations, allowing monitoring of Mg^{2+} changes in living cells without Ca^{2+} interference. It is suitable for live cell imaging with low energy excitation and is insensitive to pH changes, making it ideal for Mg^{2+} detection in a wide range of cellular environments.

However, it is inevitable that most of the above-mentioned Mg^{2+} fluorescent probes with APTRA as a binding site are single-photon fluorescent probes, which may not be able to accurately detect Mg^{2+} due to their drawbacks such as low tissue penetration depth and interference from autofluorescence. To this end, Kim *et al.* developed an innovative two-photon fluorescent probe, AMg1, capable of detecting free Mg^{2+} at a depth of several hundred micrometers in living tissue, and this design allowed AMg1 to emit strong two-photon excitation fluorescence (TPEF) when complexed with Mg^{2+}.[101] The dissociation constant (K_d) of AMg1 for Mg^{2+} is 1.6 μM, and the two-photon cross section (δ_{TPA}) of the AMg1–Mg^{2+} complex at 780 nm is 125 GM, which is seven times larger than the δ_{TPA} values of the commercial probes MgG and Mag-fura-2. The team then introduced two new two-photon fluorescence probes, FMg1 and FMg2, in combination with another probe, BCaM, which allow two-color imaging of Mg^{2+}/Ca^{2+} activity in living cells as well as imaging of the distribution in living tissue at a depth of 100–200 μm.[102,103] These probes showed high photostability in live cell imaging with minimal effect on cell activity. Using two-color imaging, the researchers were able to observe the dynamic changes in Ca^{2+} and Mg^{2+} induced by epidermal growth factor (EGF) in HepG2 cells, which is crucial for understanding the biological processes of intracellular Mg^{2+} and Ca^{2+} interactions.

A comprehensive investigation into the role of Mg^{2+} in mammalian cells has revealed that these cells undergo significant alterations in their total Mg^{2+} content when subjected to metabolic or hormonal stimulation. Conversely, the concentrations of free ions within the cytoplasm remain largely unaltered. This finding indicates the existence of organelles that dynamically regulate Mg^{2+} levels in cells. However, the currently available toolbox is insufficient for the purpose of revealing them. It is therefore imperative to develop targeted fluorescent probes to detect metal levels in specific organelles and to study patterns of ion accumulation and mobilization. To this end, D. Buccella *et al.* designed and synthesized a series of novel fluorescent probes for targeting mitochondria for the detection of free Mg^{2+} (Fig. 9a).[104] They then synthesized a targeted mitochondrial probe, Mag-mito, together with a non-targeted probe, 7c, through the introduction of a lipophilic cationic alkyl phosphate ester moiety and the enhancement of cellular membrane permeability by acetyloxymethyl ester (AM) modification. The blue shift of the fluorescence excitation maximum of probe 7c with increasing Mg^{2+} concentration demonstrated a relatively good response of the fluorescent probe to Mg^{2+} (Fig. 9b). The authors demonstrated wide-field fluorescence imaging of intracellular free Mg^{2+} in living HeLa cells treated with mitochondria-targeting Mag-mito and non-targeting control 7c. The results demonstrated that the Mag-mito probe was capable of specifically targeting and detecting free Mg^{2+} in mitochondria in living HeLa cells, whereas the non-targeting control 7c exhibited a nonspecific intracellular distribution. These data were essential for validating the tar-

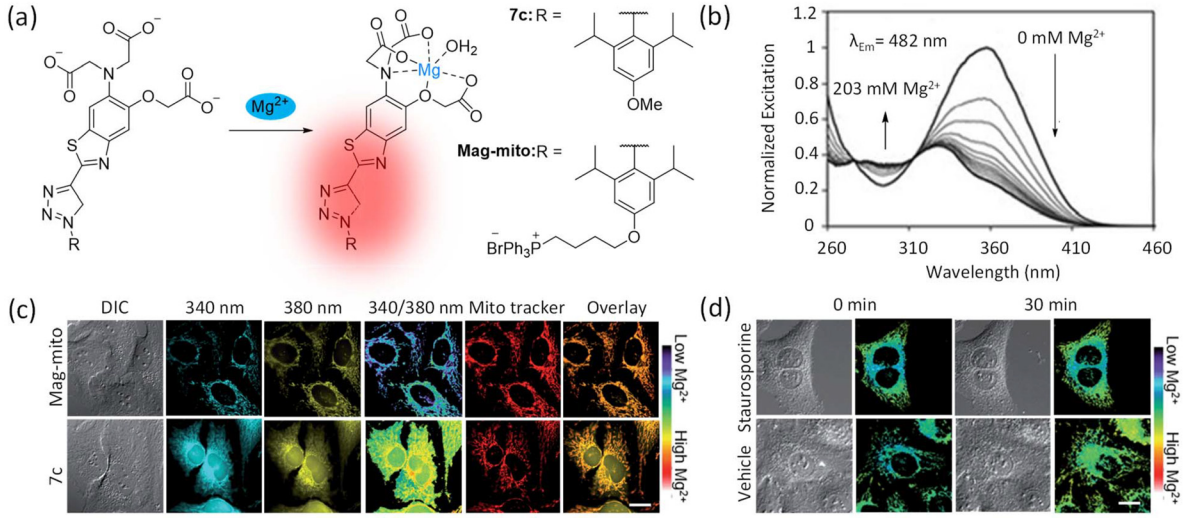

Fig. 9 Imaging and application of the mitochondria-targeted fluorescent probe Mag-mito for the detection of free Mg^{2+}. (a) Response mechanism of triazole-based fluorescent sensor to Mg^{2+}. (b) Fluorescence excitation spectra of probe 7c (2 μM) with increasing concentration of $MgCl_2$ (50 mM PIPES, 100 mM KCl, pH 7.0, 25 °C). (c) Wide-field fluorescence imaging of free Mg^{2+} in the form of acetoxymethyl ester in HeLa cells after treatment with 1 μM of Mag-mito targeting mitochondria or non-targeting control 7c. [DIC: phase contrast interferometry image; 340 nm: fluorescence under 340 nm excitation; 380 nm: fluorescence under 380 nm excitation; 340/380 nm: fluorescence ratio under 340/380 nm excitation; Mito Tracker: Mito Tracker green pseudo color in red; overlay: overlay of 380 nm channel and mitochondrial staining images]. Zoom bar = 20 μm. (d) Wide-field fluorescence imaging of mitochondrial free Mg^{2+} in live HeLa cells treated with 1 μM Mag-mito and 1 μM apoptosis-inducing staurosporine or vector. DIC images are shown with fluorescence ratiometric controls. Zoom bar = 20 μm. Reproduced with permission from ref. 104, Copyright 2015, Royal Society of Chemistry.

geting and functionality of the probe (Fig. 9c). Subsequently, the authors investigated the alterations in mitochondrial Mg^{2+} levels during staurosporine-induced apoptosis in HeLa cells and observed a significant increase in mitochondrial Mg^{2+} during the initial stages of apoptosis (Fig. 9d). This finding offers a novel insight into the function of Mg^{2+} in mitochondrial processes and apoptosis.

Nevertheless, more comprehensive design strategies for targeting imaging in other select compartments, including the nucleus and Golgi apparatus, remain scarce. Buccella *et al.* have developed a two-step strategy for the targeted anchoring of probes and *in situ* activation of fluorescent signals within specific organelles.[105] This strategy exploits bioorthogonal reactions between tetrazine-modified probes and strained alkyne hydrocarbons (with predefined localization) in genetically encoded fusion proteins to achieve precise detection of Mg^{2+} in living cells and tissues. A system combining the small molecule fluorescent probe Mag-S-Tz and the HaloTag fusion protein was designed to activate fluorescence at specific locations within the cell *via in situ* fluorescence generation reactions. This approach minimizes the accumulation of unbound fluorophores in non-targeted organelles and improves spatial resolution. In the experiments performed with HEK 293T cells, the system demonstrated its ability to comparatively assess free Mg^{2+} levels in different cellular organelles. This revealed significant disparities in Mg^{2+} levels between different organelles, highlighting the potential and applicability of this approach to explore the intracellular pathways and destinations involved in metal ion transport. Subsequently, Matsui *et al.* designed fluorescent probes for the HaloTag-coupled Mg^{2+} green derivative, MGH, which increased intracellular retention time, enabling ion imaging over extended periods and facilitating the differentiation of transient signals from sustained changes in chronic regulation.[106] These studies offer novel insights into intracellular Mg^{2+} dynamics and provide a valuable tool for developing metal ion sensing strategies targeting specific biological processes.

3.2.2 Fluorescent probes for Mg^{2+} based on charged β-diketones binding sites. Typically, the aforementioned probes with APTRA as a specific binding site result in a strong Ca^{2+} interference due to a 100-fold higher affinity for Ca^{2+} than for Mg^{2+}. In the context of these challenges, alternative receptors comprising charged β-diketones or analogous β-dicarbonyl bidentate ligand moieties have been effectively integrated into fluorescent probes for the quantification of Mg^{2+}.

Derivatives of KMG have been developed with the objective of providing high-affinity and selective detection of Mg^{2+}. The molecular design of the KMG series is based on a charged β-diketone as the Mg^{2+}-selective binding site. In 2002, Suzuki *et al.* synthesized two innovative Mg^{2+} fluorescent probes, KMG-20 and KMG-27, which are based on coumarin derivatives and incorporate a charged β-diketone structure.[107] These probes form complexes with Mg^{2+} in a 1 : 1 ratio and exhibit red-shifted absorption and fluorescence spectra with an increase in fluorescence intensity. The binding constants of these probes to Mg^{2+} are approximately 3-fold higher than those to Ca^{2+}, showing selectivity for Mg^{2+} that is more than

200-fold higher than commercially available fluorescent molecular probes for Mg^{2+} (*e.g.*, mag-fura-2 and Magnesium Green). Additionally, the fluorescence imaging of these probes in PC12 cells was demonstrated using fluorescence microscopy. When KMG-20-AM and KMG-27-AM, where AM is an acetoxymethyl ester group, were introduced into the cells, intense fluorescence was detected in the cytoplasm. In contrast, the fluorescence signal in the nucleus was significantly less pronounced. Following treatment with a high-K^+ medium, an increase in intracellular Mg^{2+} resulted in a notable enhancement in fluorescence intensity. This approach enabled the successful visualization of Mg^{2+} release from the reservoirs in real-time.

Subsequently, Komatsu *et al.* developed three fluorescein-based Mg^{2+} fluorescent probes, KMG-101, KMG-103, and KMG-104, for highly sensitive and selective imaging of intracellular Mg^{2+}.[108] KMG-103 and KMG-104 have suitable dissociation constants to increase fluorescence intensity nearly 10-fold over the 0.1–6 mM Mg^{2+} concentration range, enabling high-contrast Mg^{2+} measurements. They are 10-fold more selective for Mg^{2+} than Ca^{2+} and are insensitive to pH changes, improving the reliability of intracellular measurements. To facilitate intracellular application, the membrane-permeable probe KMG-104AM was synthesized and successfully incorporated into PC12 cells. Using confocal microscopy, the authors observed the 3D concentration distribution of Mg^{2+} in PC12 cells, confirming the effectiveness of the KMG-104 probe in cellular imaging. Using the mitochondrial uncoupler FCCP, the authors monitored changes in intracellular Mg^{2+} levels, demonstrating the potential of these probes to monitor intracellular Mg^{2+} dynamics. To investigate the mobilization and potential mechanisms of Mg^{2+}, Fujii *et al.* cleverly integrated the fluorescent probe KMG-104 into proteins and developed a novel FlAsH-type Mg^{2+} fluorescent probe, KMG-104-AsH, for specific protein labelling and detection of local changes in intracellular Mg^{2+} concentration.[109] KMG-104-AsH combines the KMG-104 and FlAsH probes to specifically bind proteins containing a tetracycline peptide tag (TCtag). In HeLa cells, the probe successfully labeled TCtag-actin and mKeima-TCtag and was able to detect concentration changes caused by FCCP-induced release of mitochondrial Mg^{2+}, demonstrating the potential to monitor Mg^{2+} dynamics in specific regions of the cell.

Extensive research has focused on the visualization of mitochondrial Mg^{2+} dynamics in living cells. To address this challenge, Shindo *et al.* developed KMG-301, a novel Mg^{2+} fluorescence probe based on a rhodamine backbone.[110] KMG-301 exhibits a 45-fold fluorescence enhancement at 100 mM Mg^{2+}, with a dissociation constant of 4.5 mM for Mg^{2+}, and is insensitive to other ions such as Ca^{2+}, Na^+, and K^+. In experiments with PC12 cells and rat hippocampal neurons, KMG-301 successfully detected a decrease in mitochondrial Mg^{2+} concentration and an increase in cytoplasmic Mg^{2+} concentration after FCCP treatment. Under conditions simulating Parkinson's disease, KMG-301 showed a gradual decrease in mitochondrial Mg^{2+} concentration, demonstrating its potential to study mitochondrial Mg^{2+} function and disease effects, and providing a new tool for understanding intracellular signaling and disease mechanisms.

While the aforementioned fluorescence has made significant advancements in the detection of Mg^{2+}, it still exhibits limitations in terms of selectivity and multicolor imaging. To this end, Murata *et al.* developed the KMG-500 series of Mg^{2+} fluorescent probes with charged β-diketones as binding sites and Si-rhodamine as a near-infrared fluorophore.[111] These probes exhibit a PET-type switching response (Fig. 10a). Two of the KMG-500 series of probes, KMG-501 and KMG-502, as well as their membrane-permeable derivatives, KMG-501AM and KMG-502AM, demonstrate high selectivity for Mg^{2+} with a K_d value of approximately 3 mM, which is suitable for detecting intracellular Mg^{2+} concentration. As an illustration, the fluorescence intensity of KMG-501 was markedly augmented with rising Mg^{2+} concentration (Fig. 10b). In cellular experiments, KMG-501AM was successfully applied to Mg^{2+} imaging of rat hippocampal neurons (Fig. 10c), demonstrating the distribution of KMG-501 within neuronal cells and its co-localization with specific intracellular organelles (*e.g.*, lysosomes and mitochondria). Furthermore, the probe was capable of detecting mitochondrial Mg^{2+} release induced by FCCP. Moreover, KMG-501 enabled the generation of multicolor imaging maps with ATP and mitochondrial membrane potential (Fig. 10d). The multicolor imaging technique allows researchers to gain a more comprehensive understanding of the interactions between intracellular Mg^{2+}, ATP concentration, and the intramitochondrial membrane potential, which is crucial for the study of cellular energy metabolism and related disease mechanisms. Similarly, the emergence of high-performance two-photon fluorescent probes based on charged beta-diketones binding sites overcomes the problems of low tissue penetration, photobleaching and phototoxicity associated with single photons. Kim *et al.* have pioneered the development of a novel two-photon fluorescent probe based on benzo[*h*]chromium derivatives, CMg1, and its derivative, CMg1-AM, for *in vivo* imaging of free Mg^{2+}.[112] The probe is capable of being excited by photons with a wavelength of 880 nm and emits strong two-photon excited fluorescence in response to Mg^{2+}. CMg1 has a water solubility of 3.0×10^{-6} M, which is suitable for cellular staining. It is pH insensitive in the biologically relevant pH range. In cellular experiments, the CMg1-AM probe was successfully employed to image Mg^{2+} in living cells (Hep3B cells) and living tissues (mouse hippocampal slices). The probe demonstrated the capacity to detect the mitochondrial-to-cytoplasmic Mg^{2+} mobilization induced by FCCP. Moreover, the CMg1 probe exhibited a two-photon excited fluorescence response in living cells that was 20 times stronger than that of existing commercial Mg^{2+} probes, including Mag-fura-2 and MgG. Additionally, it demonstrated minimal interference from Ca^{2+} ions and membrane-bound probes. This feature highlights the suitability of the probe for *in vivo* detection of Mg^{2+}.

While the KMG series of probes has been successful in reporting Mg^{2+} dynamics in living cells, the fluorescein-based

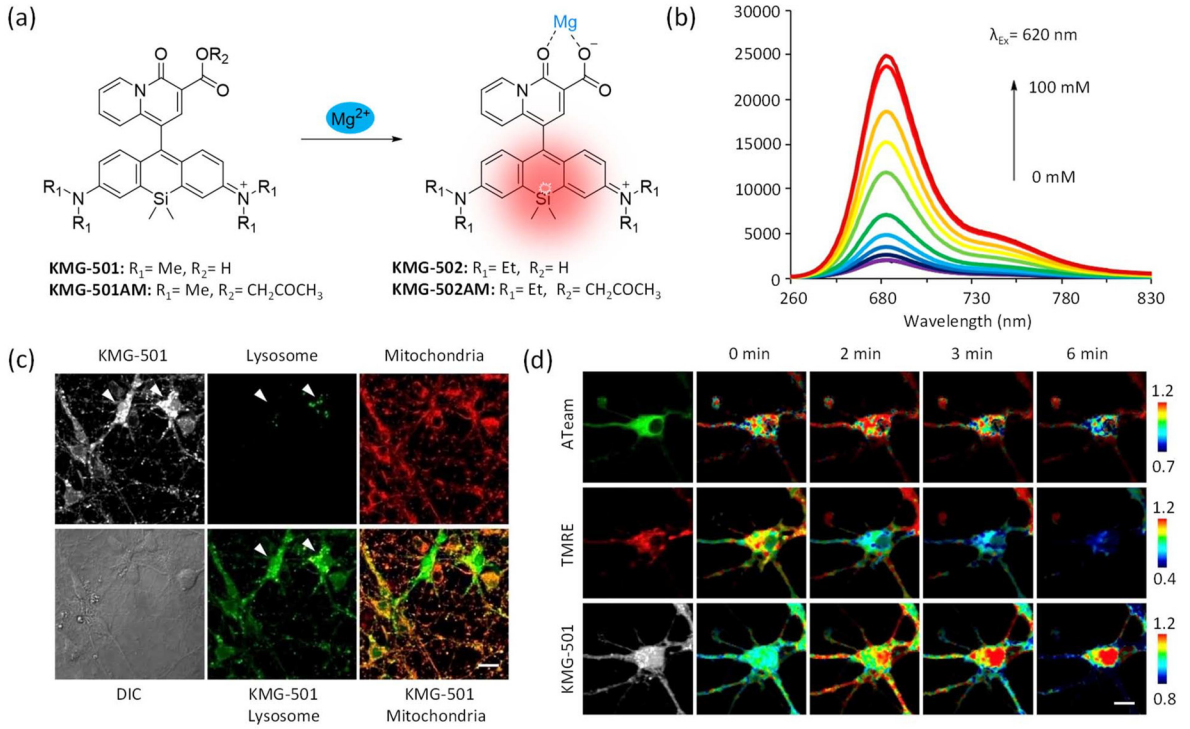

Fig. 10 Response mechanism of KMG-500 series Mg^{2+} fluorescent probes and their imaging applications in neuronal cells. (a) Response mechanism of the KMG500 series fluorescent probes to Mg^{2+}. (b) Fluorescence emission spectra of KMG-501 (5 μM) in the presence of different concentrations of Mg^{2+} (100 mM HEPES buffer, 130 mM KCl, pH 7.2, 10 mM NaCl). (c) Intracellular localization of KMG-501. [KMG-501: fluorescence images, Lysosome: Lyso Tracker Green DND-26, Mitochondria: Mito Tracker Red 580, DIC: Dlc image, KMG-501 Lysosome: merged image of KMG-501 and Lyso Tracker, KMG-501 Mitochondria: merged image of KMG-501 and Mito Tracker]. Pseudo color for each dye corresponds to the color of the caption above or below each image. Arrows indicate lysosomally bright cells. Zoom bar = 50 μm. (d) Fluorescence images of ATeam, TMRE, and KMG-501 in hippocampal neurons and false-color images at the indicated times [fluorescence ratios (R: Ch2/Ch1) were normalized by the initial ratio (*R*0) for ATeam, and fluorescence intensities *F*/*F*0 were normalized for TMRE and KMG-501]. Reproduced with permission from ref. 111, Copyright 2020, American Chemical Society.

probe KMG 104 exhibits relatively moderate turn-on ratios and low fluorescence quantum yields (Φ = 0.02) upon complexation with Mg^{2+}, which requires substantial probe loading and produces a weak signal that may be interfered with by cellular autofluorescence. The rhodamine-based analog KMG 301 demonstrated an enhanced fluorescence quantum yield (Φ = 0.15) upon Mg^{2+} binding. However, the positively charged rhodamine accumulates in mitochondria, thereby limiting the probe's utility to these organelles and precluding the detection of Mg^{2+} in other cellular compartments, including the cytoplasm. To address this shortcoming, Lin *et al.* developed novel red-emitting BODIPY-based fluorescent indicators, MagQ1 and MagQ2, for highly selective imaging of intracellular Mg^{2+}.[113] These probes introduced a 4-oxo-4*H*-quinoline-3-carboxylic acid metal-binding moiety to BODIPY for highly selective detection. MagQ1 and MagQ2 had absorption and emission peaks above 600 nm, and fluorescence intensity was enhanced 29-fold upon binding to Mg^{2+}, with quantum yields greater than 0.3. MagQ2 was improved intracellularly by the introduction of a triethylene glycol (TEG) moiety retention, reducing the active efflux of Mg^{2+} and improving the applicability of live cell imaging. MagQ2 can specifically detect Mg^{2+} at high Ca^{2+} concentrations, which is important for studying the role of Mg^{2+} in signal transduction.

3.2.3 Fluorescent probes for Mg^{2+} based on crown ether binding sites. Crown ethers, a class of macrocyclic compounds with defined cavity sizes and shapes, are capable of forming selective, stable complexes with metal ions. The most common crown ethers contain multiple ethylidene oxide units arranged in a ring-like configuration, which enables them to bind to alkali metal ions. Crown ethers have been employed extensively in the development of fluorescent probe systems due to their robust affinity for a diverse array of metal ions and chemical species.[114,115] Despite the remarkable performance of crown ethers in metal ions recognition, achieving an optimal balance between selectivity and fluorescence response in complex biological systems with a single crown ether structure remains a significant challenge. Consequently, researchers have directed their attention to 8-hydroxyquinoline (8-HQ), recognizing its exceptional chelating properties. As the second largest Mg^{2+} chelator after ethylenediaminetetraacetic acid (EDTA), 8-HQ has a low quantum yield in aqueous or organic solvents, but its binding to cations significantly enhances the fluorescence intensity.[116] Modification of 8-HQ by introducing

substituent groups not only optimizes its photophysical properties but also further enhances its selectivity for Mg^{2+}.

To integrate crown ethers with high affinity and 8-HQ with chelating properties, the research team designed and synthesized diaza-18-crown-6-ether-hydroxyquinoline (DCHQ) family fluorescent probes. The DCHQ family includes derivatives such as DCHQ1, DCHQ2, DCHQ3, DCHQ4, DCHQ5, and DCHQ6 (Table 1), which enhance affinity, cellular uptake, membrane staining, and fluorescence response to Mg^{2+} by introducing different groups (*e.g.*, hydrogen atoms, chlorine atoms, acetoxymethyl ester groups, long alkyl chains, and aromatic groups) into the side arm of 8-hydroxyquinoline.[117–121] These enhancements render DCHQ probes more efficacious and selective in biomedical research, particularly in the case of DCHQ5, which exhibits distinctive fluorescence characteristics and an exceptional capacity for intracellular retention, thereby conferring upon it a formidable capability for investigating Mg^{2+} distribution and homeostasis.

Two compounds belonging to the DCHQ family, DCHQ1 and DCHQ2, display a markedly elevated affinity for Mg^{2+}, exceeding that of other commercially available Mg^{2+} probes. These compounds do not cross-react with other divalent cations, including Ca^{2+}, even within the physiological pH range. DCHQ1 is well tolerated by cells and can be used to quantitatively assess total intracellular Mg^{2+} content *via* a simple spectrofluorimetric assay. The fluorescence signal of DCHQ1 correlates with the cellular Mg^{2+} content and is sufficiently sensitive to distinguish changes in Mg^{2+} content in trace samples. Despite its potential, the excitation of DCHQ1 in the UV region and incomplete intracellular retention limit its effectiveness as a leading probe in the DCHQ family. In comparison to DCHQ1, DCHQ5 exhibits enhanced fluorescence intensity, stronger membrane staining, and superior intracellular retention when binding to cations. Additionally, DCHQ5 fluorescence is not significantly influenced by other divalent cations or by physiological range pH alterations. The detection limit of the probe is comparable to that of flame atomic absorption spectroscopy (F-AAS), which is 0.2 mM, rendering it suitable for analytical experiments. DCHQ5 is able to accurately quantify the total amount of intracellular Mg^{2+} even in sample sizes much smaller than those required for F-AAS (*e.g.*, 50 000 cells), suggesting that DCHQ5 has the potential to be a powerful tool for revealing the regulatory mechanism of Mg^{2+} in cellular homeostasis.

3.2.4 Fluorescent probes for Mg^{2+} based on Schiff base ligands binding site. Schiff bases are a class of compounds containing C=N double bonds, which are simple to synthesize and easy to derivatize. Furthermore, they can be chelated with metal ions to form "planar, rigid, and large conjugated π-bonds" with fluorescence characteristics. In particular, when Schiff base compounds are coordinated with metal ions, the C=N double bonds exhibit different configurations, resulting in changes in the spectra. This enables selective recognition of specific ions or molecules. Consequently, the synthesis of metal ion probes by incorporating fluorescent groups into Schiff base compounds has garnered significant interest from the scientific community.[122]

For example, Orrego-Hernández *et al.* developed a novel Mg^{2+} fluorescence "turn-on" probe, PyHC, which is based on a pyridyl-hydrazino-coumarin structure.[123] The PyHC probe exhibits significant fluorescence enhancement of Mg^{2+} in ethanol–water solution, with a low detection limit of 105 nM. This fluorescence enhancement is attributed to the coordination with Mg^{2+}, which increases structural rigidity and suppresses non-radiative decay processes. It was demonstrated that PyHC displays a high affinity for Mg^{2+} with a binding constant of 5.57×10^4 L mol^{-1} and exhibits minimal interference from Ca^{2+}.

While progress has been made with single detection probes for Mg^{2+}, multifunctional probes are of interest due to their ability to detect multiple analytes simultaneously. This direction is exemplified by the chalcone backbone probes L_a and L_b reported by Yadav *et al.*[124] The L_a probe is responsive to both Mg^{2+} and Mn^{2+}, whereas L_b selectively binds Cu^{2+} and Mg^{2+}. The detection limits of both for Mg^{2+} reached 2.56×10^{-6} M and 1.28×10^{-6} M, respectively, while (3-(4,5-dimethyl-2-thiazolyl)-2,5-diphenyl-2*H*-tetrazolium bromide) (MTT) experiments showed that these probes and their Mg^{2+} complexes showed low cytotoxicity against the HeLa cancer cell line and showed good biocompatibility. Although both showed the ability to detect a wide range of analytes, they were mainly used for Mg^{2+} detection.

Singh *et al.* developed a fluorescent probe, HL ((*E*)-8-((benzo[*d*]thiazol-2-ylimino)methyl)-7-hydroxy-4-methyl-2*H*-chromen-2-one), for the simultaneous detection of Mg^{2+} and Zn^{2+}.[125] HL

Table 1 Basic photophysical properties of the fluorescent Mg^{2+} probes based on crown ether binding site

Compound	λ_{max} (λ_{abs})/nm	λ_{max} (λ_{em})/nm	ε/cm^{-1} M^{-1}	Φ	log K_a			Imaging targets	Ref.
					Mg^{2+}	Zn^{2+}	Cd^{2+}		
DCHQ1	244 (244)	505 (505)	6.5×10^4	2.3×10^{-2}	5.02 ± 0.08^a	5.85 ± 0.06^a	9.39 ± 0.05^b	HC11 cells, HL60cells	117
DCHQ2	245 (245)	510 (510)	—	—	—	—	—	HC11 cells	117
DCHQ3	246 (246)	510 (513)	1.29×10^5	7.7×10^{-3}	10.1 ± 0.10^b	6.12 ± 0.07^a	9.53 ± 0.05^b	HL60cells	118
DCHQ4	247 (247)	463 (513)	1.32×10^5	6.7×10^{-3}	11.2 ± 0.40^b	6.50 ± 0.20^a	9.30 ± 0.06^b	HL61cells	119
DCHQ5	249 (249)	512 (517)	6.6×10^4	2.4×10^{-2}	5.08 ± 0.06^a	6.60 ± 0.20^a	9.40 ± 0.20^b	HL62cells	120
DCHQ6	245 (245)	504 (514)	9.2×10^4	9.8×10^{-3}	4.80 ± 0.40^a	5.80 ± 0.09^a	8.91 ± 0.06^b	HL63cells	121

[a] Value obtained for 1 : 1 metal-to-ligand stoichiometry. [b] Value obtained for a 1 : 2 metal-to-ligand stoichiometry. If not otherwise stated, K_a values were measured in aqueous buffers; for details, please see the cited references.

has a large Stokes shift, allowing it to discriminate between the two ions at 483 nm and 560 nm. It achieves high sensitivity detection by inhibiting C=N bond rotation and photoinduced electron transfer (PET) and excited state intramolecular proton transfer (ESIPT) while promoting chelation enhanced fluorescence (CHEF). HL has a fast and reversible fluorescence response to Mg^{2+} and Zn^{2+} with a low detection limit and high binding constants. In human breast cancer cells, HL can also successfully distinguish between Mg^{2+} and Zn^{2+}. The study also explored the potential application of HL in practical sample detection and low-cost methods. Density Functional Theory (DFT) calculations simulated the binding modes of HL to Mg^{2+} and Zn^{2+}, further confirming the high selectivity and sensitivity of the probe.

3.2.5 Fluorescent probes for Mg^{2+} based on 2,8-dicarboxyquinoline binding site. While the β-diketone and KMG series probes, characterized by their bidentate chelating sites, are known for their selectivity towards Mg^{2+}, they show minimal binding to Ca^{2+}, as reflected in their millimolar dissociation constants. However, it is difficult for the bidentate ligands to distinguish between free Mg^{2+} and Mg-ATP complex, which is the most abundant form of Mg^{2+} in the cell.[126] Consequently, Matsui *et al.* devised a three-dentate Mg^{2+} chelator, 2,8-dicarboxyquinoline (DCQ), by modifying the dimensions of the rigid cavity within the chelator section.[127] Based on this Mg^{2+} chelator, they constructed fluorescent probes, MGQ1 and MGQ2, for the visualization of intracellular Mg^{2+} dynamics while circumventing the interference of Ca^{2+} fluctuations. MGQ-1 operates *via* a PET mechanism with an appropriate affinity for Mg^{2+} (K_d = 0.14 mM). However, its fluorescence intensity is affected by pH changes. MGQ-2 reduces pH sensitivity by introducing a chlorine atom at position 6 of the DCQ, resulting in a higher affinity for Mg^{2+} (K_d = 0.27 mM). MGQ-2 demonstrated a significantly lower affinity for Ca^{2+} (K_d = 1.5 mM) and a notable degree of photostability and nuclear localization in living cells. Furthermore, the fluorescence intensity remained unaltered during Ca^{2+} influx, indicating its specificity for Mg^{2+}. These probes offer novel tools for investigating the function of Mg^{2+} in cells, particularly in organelles with elevated Ca^{2+} concentrations, and facilitate the elucidation of the hitherto unknown role of Mg^{2+} in cellular physiological processes.

Subsequently, in 2023, the team combined MGQ-2 and a HaloTag ligand to develop the fluorescent probe MGQ-2H for specific and long-term subcellular localization.[128] The probe is stable in a neutral pH range and exhibits minimal sensitivity to pH fluctuations. However, it displays a notable decline in fluorescence intensity under acidic conditions. In HEK293 cells, MGQ-2H was successfully localized to the nucleus, cytoplasm, and inner leaflet of the cell membrane. MGQ-2H demonstrated high selectivity for Mg^{2+} with an apparent K_d of 0.23 mM, compared to a K_d of 1.1 mM for Ca^{2+}. By employing

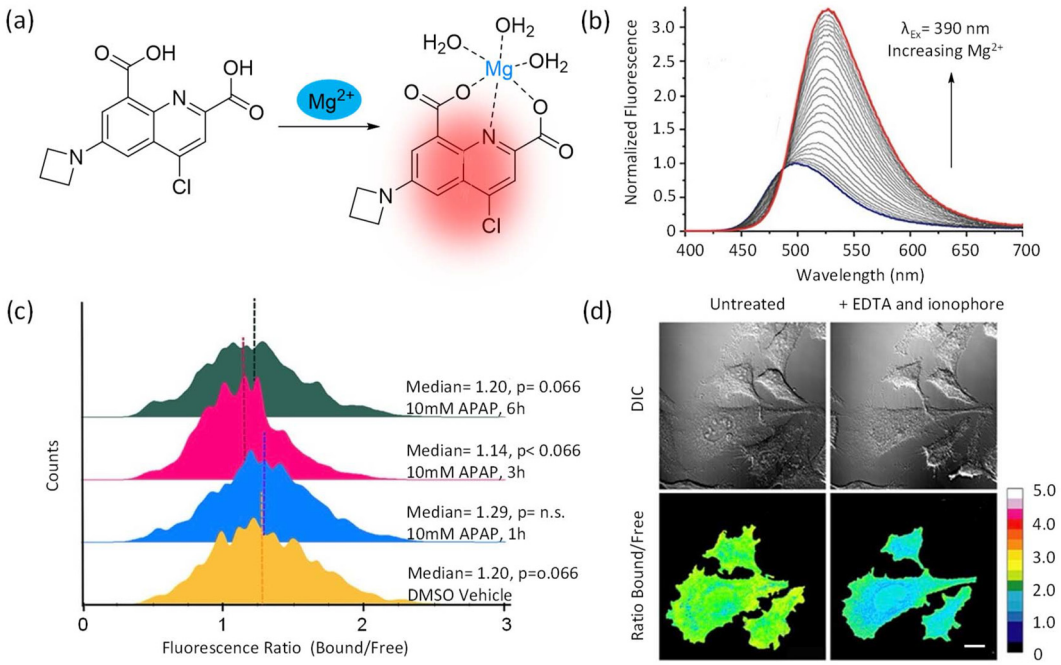

Fig. 11 MagZet1 fluorescent probe for Mg^{2+} detection and its application in cellular models of APAP-induced liver injury. (a) Response mechanism of fluorescent probe MagZet1 to Mg^{2+}. (b) Fluorescence emission spectra of MagZet1 (10 μM) with increasing Mg^{2+} concentration (50 mM PIPES, 100 mM KCl, pH 7.0). (c) Flow cytometry histograms showing the MagZet1 fluorescence ratios of THLE-2 cells treated with DMSO vector (yellow) or 10 mM acetaminophen (APAP) for 1 h (blue), 3 h (red), or 6 h (green). Dashed lines represent median fluorescence ratios. *p*-Values were calculated based on the chi-square values of the corresponding populations compared with DMSO-treated controls. (d) Fluorescence images of HeLa cells stained with MagZet1-AM (5 μM) before and after treatment with the ion carrier 4-Br-A-23187 and EDTA. Zoom bar = 25 μm. Reproduced with permission from ref. 132, Copyright 2023, American Chemical Society.

ratiometric fluorescence microscopy techniques with the internal standard HTL-Sara650T, MGQ-2H was able to successfully visualize the alterations in Mg^{2+} concentration within the nucleus during mitosis. The findings revealed that the Mg^{2+} concentration reached its peak at the mid-stage of mitosis and subsequently recovered to its initial level before the onset of cytoplasmic division. MGQ-2H displays good intracellular stability and is suitable for observing Mg^{2+} dynamics over extended periods. However, it should be noted that the probe exhibits fluorescence bursting property under acidic conditions and displays a relatively high affinity for Fe^{2+} and Zn^{2+}. Notwithstanding these constraints, MGQ-2H offers a novel avenue for investigating intracellular Mg^{2+} dynamics, particularly in the context of concurrent Ca^{2+} fluctuations.

It is noteworthy that analogous targeted strategies have been employed in the subcellular detection of other metal ions.[129] For instance, the trivalent metal ion sensor developed by Koner *et al.* facilitates specific bioimaging and quantitative detection of aluminium ions (Al^{3+}) in lysosomes, providing a novel instrument for the study of the subcellular distribution of metal ions.[130] Subsequently, in 2024, the team published a comprehensive review of the field of lysosomal metal ion detection, systematically summarising the design strategies for fluorescent probes targeting iron, copper, zinc, potassium, calcium, and other ions.[131] These probes achieve lysosomal localization through the modification of lipophilic amine groups or specific membrane protein ligands, thereby providing critical technical support for exploring the role of metal ions in cellular metabolism and pathological processes.

Flow cytometry is a powerful technique that offers significant advantages, including high-throughput analysis, the ability to measure multiple parameters, and the capacity to assess single cells. Consequently, Brady *et al.* developed MagZet1, a scaled fluorescent probe based on 2,8-dicarboxyquinoline (Fig. 11a).[132] Flow cytometry analysis was performed to reveal the decrease in cytoplasmic Mg^{2+} levels in a cellular model of acetaminophen (APAP)-induced liver injury. The fluorescent properties of MagZet1 undergo a significant alteration upon binding of Mg^{2+}, with the absorption peak shifting from 490 nm to 395 nm, and the fluorescence emission peak shifting from 500 nm to 530 nm (Fig. 11b). Furthermore, the fluorescence ratio of MagZet1 remains largely unaffected by pH

Table 2 Basic characteristics of Mg^{2+} fluorescent probes

Probes	λ_{ex}/nm	λ_{em}/nm	K_d/mM	Cell	Localization	Ref.
APTRA-based probes						
Mag–S	392	547	3.2	HeLa cells	Cytoplasm, some organelles	98
Mag–Se	410	562	3.3	—	—	98
MagB1	496	508	4.3	—	—	100
MagB2	575	601	2.13	HeLa cells	Cytoplasm	100
AMg1	365	498	1.4	Hep3B cells	—	101
FMg1	360	540	1.5	HepG2 cells	—	102
FMg2	368	555	1.7	HepG2 cells	—	102
Mag-mito	356	495	6.7	HeLa cells	Mitochondria	104
Mag-S-Tz	404	595	3.1	HEK 293T cells	Cytoplasm, nuclei, Golgi	105
MGH	515	538	1.3	HEK 293T cells	Nuclei, innercell membrane, Cyto plasm, ER, Mito chondria	106
Charged β-diketone-based probes						
KMG-20	445	495	10	PC12 cells	Cytoplasm	107
KMG-27	445	494	9.8	PC12 cells	Cytoplasm	107
KMG-101	493	516	100	PC12 cells	—	108
KMG-103	517	533	1.8	PC12 cells	—	108
KMG-104	504	523	2.1	PC12 cells	Cytoplasm	108
KMG-104-AsH	490	540	1.7	HeLa cells	—	109
KMG-301	540	600	4.5	PC12 cells	Mitochondria	110
KMG-501	663	684	3.2	PC12 cells	Cytoplasm, mitochondria, lysosome	111
KMG-502	670	690	2.6	PC12 cells	—	111
CMg1	443	559	1.3	Hep3B cells	—	112
MagQ1	600	635	1.5	HeLa cells	Cytoplasm, nuclei	113
MagQ2	600	634	1.51	HeLa cells		114
Schiff-based probes						
PyHC	340	449	5.57	—	—	123
La	382	526	1.2	HeLa cells	—	124
HL	451	483	—	MDA-MB cells	Cytoplasm	125
2,8-Dicarboxyquinoline-based probes						
MGQ1	515	536	0.14	—	—	126
MGQ2	516	536	0.26	HEK293 cells	Cytoplasm, nuclei	127
MGQ-2H	524	545	0.23	HEK293 cells	Cytoplasm, nuclei	128
MagZet1	395	530	0.14	THLE-2 cells	Cytoplasm	132

For details, please see the cited references.

fluctuations within the physiological range, which is a crucial attribute in bioimaging applications. MagZet1 also exhibits a reduced proclivity to form ternary complexes, thereby reducing the likelihood of interference in the detection of Mg^{2+} in biological samples. For the purpose of live cell imaging, MagZet1 is capable of detecting Mg^{2+} by means of fluorescence microscopy and flow cytometry. In HeLa cells, MagZet1-AM, in which the probe was converted to the acetoxymethyl ester form, exhibited uniform cytoplasmic staining, indicating that it was effectively distributed within the cell (Fig. 11d). Researchers employed flow cytometry to examine changes in Mg^{2+} levels in APAP-treated hepatocytes. They found that in a cellular model of APAP-induced liver injury, the reduction in intracellular free Mg^{2+} levels was linked to altered expression of the metal transporter protein CNNM4 (Fig. 11c).

The development of MagZet1 provides a novel tool for investigating the function of Mg^{2+} in cells, particularly in contexts where Ca^{2+} levels may be altered. The selectivity of this probe is of paramount importance for studying systems that may be affected by Ca^{2+} levels, as it can reveal the intricate interactions between these two ions. The introduction of MagZet1 is anticipated to provide novel insights into the study of Mg^{2+} in other systems.

In summary, the various Mg^{2+} fluorescent probes developed in recent years have different focuses in terms of selectivity, sensitivity, and application scenarios. The purpose of this work is to systematically compare the key performance parameters of the relevant probe types. A series of fluorescent probes have been developed and their characteristics (*e.g.* K_d, excitation/emission wavelengths, and applicable scenarios) are shown in Table 2. This review provides a reference for researchers to select suitable probe tools according to their experimental needs.

4. Conclusions

In recent years, significant advancements have been made in elucidating the mechanistic roles of Mg^{2+} in human homeostasis. However, compared to other biologically relevant metal ions, our understanding of Mg^{2+} remains incomplete. This review systematically delineates the intricate relationship between Mg^{2+} and biological systems, emphasizing its fundamental physiological roles as a structural stabilizer and enzymatic cofactor. Dysregulation of Mg^{2+} homeostasis has been linked to multiple pathological conditions, including hypertension, metabolic disorders, and neurodegeneration, underscoring the necessity for precise analytical methodologies. The review further evaluates established techniques for Mg^{2+} detection, which have deepened insights into its physiological and pathological mechanisms. Current detection strategies exhibit critical trade-offs among sensitivity, selectivity, and practical utility. Non-fluorescent approaches such as AAS and electrochemical sensors demonstrate high accuracy but lack the spatial resolution required for dynamic cellular tracking. While fluorescent probes enable real-time imaging with temporal resolution, their performance is compromised by interference (*e.g.*, Ca^{2+} cross-reactivity) and limited tissue penetration depth. Future research must prioritize the development of probes with enhanced selectivity in complex biological matrices, improved real-time monitoring capabilities, and clinically translatable platforms for personalized therapeutics. Addressing these challenges will bridge the gap between mechanistic insights and therapeutic applications, ultimately advancing diagnostic precision and tailored treatment strategies for Mg^{2+}-associated disorders.

Abbreviations

AAS	Atomic absorption spectrometry
ACoA	Acetyl Coenzyme A
AM	Acetoxymethyl ester
APTRA	*o*-Aminophenol-*N*,*N*,*O*-triacetic acid
ASEM	Analytical scanning electron microscopy
ATP	Adenosine triphosphate
BBB	Blood–brain barrier
BODIPY	Boron-dipyrromethene
Ca^{2+}	Calcium ions
CAR-T	Chimeric antigen receptor T-cell
CNS	Central nervous system
DBP	Vitamin D-binding protein
DCQ	2,8-Dicarboxyquinoline
DCHQ	Diaza-18-crown-6-ether-hydroxyquinoline
DFT	Density functional theory
eNOS	Endothelial nitric oxide synthase
EDS	Energy dispersive X-ray spectroscopy
EDTA	Ethylenediaminetetraacetic acid
EGF	Epidermal growth factor
EMIM-Ac	1-Ethyl-3-methylimidazolium acetate
ESIPT	Excited-state intramolecular proton transfer
F-AAS	Flame atomic absorption spectroscopy
FCCP	Carbonyl cyanide-4-(trifluoromethoxy) phenylhydrazone
GABA	Gamma-aminobutyric acid
G6PD	Glucose-6-phosphate dehydrogenase
IL-4	Interleukin-4
ISEs	Ion-selective electrodes
K^+	Potassium ions
LFA-1	Lymphocyte function-associated antigen-1
Mg^{2+}	Magnesium ions
MTT	3-(4,5-Dimethyl-2-thiazolyl)-2,5-diphenyl-2*H*-tetrazolium bromide
Na^+	Sodium ions
NCX	Sodium-calcium exchanger
NMDA	*N*-Methyl-D-aspartate
NMR	Nuclear magnetic resonance
NO	Nitric oxide
OGDH	α-Ketoglutarate dehydrogenase complex
OXPHOS	Oxidative phosphorylation
PDB	Protein data bank
PDH	Pyruvate dehydrogenase

PET	Photoinduced electron transfer
PIXE	Particle-induced X-ray emission
PTH	Parathyroid hormone
PVC	Polyvinyl chloride
ROS	Reactive oxygen species
rRNA	Ribosomal RNA
SERCA	Sarcoplasmic/endoplasmic reticulum calcium ATPase
SLC41A3	Solute carrier family 41 member A3
SXRF	Synchrotron X-ray fluorescence
TCtag	Tetracysteine tag
TLR	Toll-like receptor
TMRE	Tetramethylrhodamine ethyl ester
TPEF	Two-photon excitation fluorescence
TRPM7	Transient receptor potential melastatin 7
tRNA	Transfer RNA
VDR	Vitamin D receptor
XRF	X-ray fluorescence
XMEN	X-linked immunodeficiency with magnesium deficiency, EBV infection, and neoplasia

Author contributions

Tianwei Liu: investigation, data curation, formal analysis, writing of original draft (equal contribution); Lan Wang: validation, formal analysis, writing of original draft (equal contribution); Siying Pei: investigation (supporting contribution); Shuo Yang: validation (supporting contribution); Jiayi Wu: supervision (supporting contribution); Wei Liu: project administration, funding acquisition (supporting contribution); Qiong Wu: project administration, funding acquisition (supporting contribution).

Conflicts of interest

The authors declare that they have no known competing financial interests or personal relationships that could have appeared to influence the work reported in this paper.

Data availability

All relevant data are included in the manuscript.

Acknowledgements

This work was financially supported by the National Natural Science Foundation of China (62288102), Scientific and Technological Project of Henan Province (252102211093), the Project of Henan Institute of Flexible Electronics (HIFE), and Postgraduate Research & Practice innovation Program of Jiangsu Province (KYCX22_1337).

References

1 M. E. Maguire and J. A. Cowan, *BioMetals*, 2002, **15**, 203–210.
2 A. M. P. Romani, *Arch. Biochem. Biophys.*, 2011, **512**, 1–23.
3 F. I. Wolf and V. Trapani, *Clin. Sci.*, 2008, **114**, 27–35.
4 J. H. F. de Baaij, J. G. J. Hoenderop and R. J. M. Bindels, *Physiol. Rev.*, 2015, **95**, 1–46.
5 C. G. Musso, *Int. Urol. Nephrol.*, 2009, **41**, 357–362.
6 G. Picone, C. Cappadone, G. Farruggia, E. Malucelli and S. Iotti, *Magnesium Res.*, 2020, **33**, 1–11.
7 N. I. Georgiev, V. V. Bakov, K. K. Anichina and V. B. Bojinov, *Pharmaceutics*, 2023, **16**, 381.
8 L. M. Resnick, M. Barbagallo, L. J. Dominguez, J. M. Veniero, J. P. Nicholson and R. K. Gupta, *Hypertension*, 2001, **38**, 709–712.
9 M. Pelczyńska, M. Moszak and P. Bogdański, *Nutrients*, 2022, **14**, 1714.
10 S. Johnson, *Med. Hypotheses*, 2001, **56**, 163–170.
11 T. Dyckner, B. Ek, H. Nyhlin and P. O. Wester, *Acta Med. Scand.*, 1985, **218**, 129–131.
12 F. I. Bussière, E. Gueux, E. Rock, J. P. Girardeau, A. Tridon, A. Mazur and Y. Rayssiguier, *Br. J. Nutr.*, 2002, **87**, 107–113.
13 J. Sugimoto, A. M. Romani, A. M. Valentin-Torres, A. A. Luciano, C. M. Ramirez Kitchen, N. Funderburg, S. Mesiano and H. B. Bernstein, *J. Immunol.*, 2012, **188**(63), 38–6346.
14 S. Feske, E. Y. Skolnik and M. Prakriya, *Nat. Rev. Immunol.*, 2012, **12**, 532–547.
15 C. Montell, *Curr. Biol.*, 2003, **13**, R799–R801.
16 F. Jin, Y. Huang and M. Hattori, *J. Mol. Biol.*, 2022, **434**, 167729.
17 C. Schmitz, A. L. Perraud, C. O. Johnson, K. Inabe, M. K. Smith, R. Penner, T. Kurosaki, A. Fleig and A. M. Scharenberg, *Cell*, 2003, **114**, 191–200.
18 W. Nadolni and S. Zierler, *Cells*, 2018, **7**, 109.
19 J. Lötscher, A. A. M. I. Lindez, N. Kirchhammer, E. Cribioli, G. M. P. G. Attianese, M. P. Trefny, M. Lenz, S. I. Rothschild, P. Strati, M. Kuenzli, C. Lotter, S. H. Schenk, P. Dehio, J. Loeliger, L. Litzler, D. Schreiner, V. Koch, N. Page, D. Lee, J. Graehlert, D. Kuzmin, A. V. Burgener, D. Merkler, M. Pless, M. L. Balmer, W. Reith, J. Huwyler, M. Irving, C. G. King, A. Zippelius and C. Hess, *Cell*, 2022, **185**, 585–602.
20 F. J. Rios, Z. G. Zou, A. P. Harvey, K. Y. Harvey, R. Nosalski, P. Anyfanti, L. L. Camargo, S. Lacchini, A. G. Ryazanov, L. Ryazanova, S. McGrath, T. J. Guzik, C. S. Goody, A. C. Montezano and R. M. Touyz, *Cardiovasc. Res.*, 2020, **116**, 721–735.
21 T. Schilling, F. Miralles and C. Eder, *J. Cell Sci.*, 2014, **127**, 4561–4566.
22 F. Y. Li, B. Chaigne-Delalande, C. Kanellopoulou, J. C. Davis, H. F. Matthews, D. C. Douek, J. I. Cohen, G. Uzel, H. C. Su and M. J. Lenardo, *Nature*, 2011, **475**, 471–476.

23 F. Y. Li, M. J. Lenardo and B. Chaigne-Delalande, *Magnesium Res.*, 2011, **24**, S109–S114.
24 K. Tangvoraphonkchai and A. Davenport, *Adv. Chronic Kidney Dis.*, 2018, **25**, 251–260.
25 K. Mubagwa, A. Gwanyanya, S. Zakharov and R. Macianskiene, *Arch. Biochem. Biophys.*, 2007, **458**, 73–89.
26 R. E. White and H. C. Hartzell, *Science*, 1988, **239**, 778–780.
27 S. Brunet, T. Scheuer, R. Klevit and W. A. Catterall, *J. Gen. Physiol.*, 2005, **126**, 311–323.
28 M. Wang, M. Tashiro and J. R. Berlin, *J. Physiol.*, 2004, **555**, 383–396.
29 I. Duchatelle-Gourdon, H. C. Hartzell and A. A. Lagrutta, *J. Physiol.*, 1989, **415**, 251–274.
30 B. A. Williams and G. N. Beatch, *Am. J. Physiol.*, 1997, **272**, H1292–H1301.
31 G. Z. Sudo and M. C. Sanguinetti, *J. Pharmacol. Exp. Ther.*, 1996, **276**, 951–957.
32 A. P. Michailova, M. E. Belik and A. D. McCulloch, *J. Am. Coll. Nutr.*, 2004, **23**, 514S–517S.
33 L. Boyman, H. Mikhasenko, R. Hiller and D. Khananshvili, *J. Biol. Chem.*, 2009, **284**, 6185–6193.
34 V. Breukels, A. Konijnenberg, S. M. Nabuurs, W. G. Touw and G. W. Vuister, *Biochemistry*, 2011, **50**, 8804–8812.
35 J. Ma, N. Zhao and D. Zhu, *J. Biomed. Mater. Res., Part A*, 2016, **104**, 347–356.
36 P. Severino, L. Netti, M. V. Mariani, A. Maraone, A. D'Amato, R. Scarpati, F. Infusino, M. Pucci, C. Lavalle, V. Maestrini, M. Mancone and F. Fedele, *Cardiol. Res. Pract.*, 2019, **2019**, 4874921.
37 M. Houston, *J. Clin. Hypertens.*, 2011, **13**, 843–847.
38 M. H. Salimi, J. C. Heughebaert and G. H. Nancollas, *Langmuir*, 1985, **1**, 119–122.
39 T. Vetter and M. J. Lohse, *Curr. Opin. Nephrol. Hypertens.*, 2002, **11**, 403–410.
40 S. Erem, A. Atfi and M. S. Razzaque, *J. Steroid Biochem. Mol. Biol.*, 2019, **193**, 105400.
41 I. Hendrix, P. Anderson, B. May and H. Morris, *J. Steroid Biochem. Mol. Biol.*, 2004, **89–90**, 139–142.
42 S. Ozsoylu and N. Hanioglu, *Turk. J. Pediatr.*, 1977, **19**, 89–96.
43 S. M. Greising, H. M. Gransee, C. B. Mantilla and G. C. Sieck, *Wiley Interdiscip. Rev.:Syst. Biol. Med.*, 2012, **4**, 457–473.
44 R. Yamanaka, S. Tabata, Y. Shindo, K. Hotta, K. Suzuki, T. Soga and K. Oka, *Sci. Rep.*, 2016, **6**, 30027.
45 L. Garfinkel and D. Garfinkel, *Magnesium*, 1985, **4**, 60–72.
46 I. Pilchova, K. Klacanova, Z. Tatarkova, P. Kaplan and P. Racay, *Oxid. Med. Cell. Longevity*, 2017, **2017**, 6797460.
47 M. A. Galkin and A. V. Syroeshkin, *Biochemistry*, 1999, **64**, 1176–1185.
48 F. Sun, Z. Zhao, M. M. Willoughby, S. Shen, Y. Zhou, Y. Shao, J. Kang, Y. Chen, M. Chen, X. Yuan, I. Hamza, A. R. Reddi and C. Chen, *Nature*, 2022, **610**, 768–774.
49 L. M. Guthrie, S. Soma, S. Yuan, A. Silva, M. Zulkifli, T. C. Snavely, H. F. Greene, E. Nunez, B. Lynch, C. De Ville, V. Shanbhag, F. R. Lopez, A. Acharya, M. J. Petris, B.-E. Kim, V. M. Gohil and J. C. Sacchettini, *Science*, 2020, **368**, 620–625.
50 J. S. Rodriguez-Zavala and R. Moreno-Sánchez, *J. Biol. Chem.*, 1998, **273**, 7850–7855.
51 B. Barbiroli, S. Iotti, P. Cortelli, P. Martinelli, R. Lodi, V. Carelli and P. Montagna, *J. Cereb. Blood Flow Metab.*, 1999, **19**, 528–532.
52 J. A. Maier, S. Castiglioni, L. Locatelli, M. Zocchi and A. Mazur, *Semin. Cell Dev. Biol.*, 2021, **115**, 37–44.
53 L. V. Kalia, S. K. Kalia and M. W. Salter, *Lancet Neurol.*, 2008, **7**, 742–755.
54 T. Möykkynen, M. Uusi-Oukari, J. Heikkilä, D. M. Lovinger, H. Lüddens and E. R. Korpi, *NeuroReport*, 2001, **12**, 2175–2179.
55 V. Romeo, A. Cazzaniga and J. A. M. Maier, *Magnesium Res.*, 2019, **32**, 16–24.
56 S. M. Hancock, D. I. Finkelstein and P. A. Adlard, *Front. Aging Neurosci.*, 2014, **6**, 137.
57 J. Olloquequi, E. Cornejo-Córdova, E. Verdaguer, F. X. Soriano, O. Binvignat, C. Auladell and A. Camins, *J. Psychopharmacol.*, 2018, **32**, 265–275.
58 J. Anastassopoulou and T. Theophanides, *Crit. Rev. Oncol. Hematol.*, 2002, **42**, 79–91.
59 J. Wang and Y. Xiao, *Phys. Rev. E*, 2016, **94**, 040401.
60 J. C. Bowman, T. K. Lenz, N. V. Hud and L. D. Williams, *Curr. Opin. Struct. Biol.*, 2012, **22**, 262–272.
61 H. Pelletier, M. R. Sawaya, A. Kumar, S. H. Wilson and J. Kraut, *Science*, 1994, **264**, 1891–1903.
62 R. Yamagami, J. P. Sieg and P. C. Bevilacqua, *Biochemistry*, 2021, **60**, 2374–2386.
63 F. I. Wolf, J. A. M. Maier, A. Nasulewicz, C. Feillet-Coudray, M. Simonacci, A. Mazur and A. Cittadini, *Arch. Biochem. Biophys.*, 2007, **458**, 24–32.
64 D. Forrest, *Biochem. Soc. Trans.*, 2018, **47**, 219–228.
65 G. Akanuma, *Biosci. Biotechnol. Biochem.*, 2021, **85**, 1582–1593.
66 C. Sara and A. M. M. Jeanette, *Magnesium Res.*, 2011, **24**, 92–100.
67 M. E. Rodríguez-Ortiz, A. Canalejo, C. Herencia, J. M. Martínez-Moreno, A. Peralta-Ramírez, P. Perez-Martinez, J. F. Navarro-González, M. Rodríguez, M. Peter, K. Gundlach, S. Steppan, J. Passlick-Deetjen, J. R. Muñoz-Castañeda and Y. Almaden, *Nephrol., Dial., Transplant.*, 2014, **29**, 282–289.
68 L. Lvova, C. G. Gonçalves, C. Di Natale, A. Legin, D. Kirsanov and R. Paolesse, *Talanta*, 2018, **179**, 430–441.
69 G. D. Christian, *Anal. Chem.*, 1969, **41**, 24A–40A.
70 V. Ugurlu, C. Binay, E. Simsek and C. Bal, *J. Clin. Res. Pediatr. Endocrinol.*, 2016, **8**, 180–186.
71 H. Millart, V. Durlach and J. Durlach, *Magnesium Res.*, 1995, **8**, 65–76.
72 E. S. Dipietro, M. M. Bashor, P. E. Stroud, B. J. Smarr, B. J. Burgess, W. E. Turner and J. W. Neese, *Sci. Total Environ.*, 1988, **74**, 249–262.
73 K. Schilling, F. Larner, A. Saad, R. Roberts, H. M. Kocher, O. Blyuss, A. N. Halliday and T. Crnogorac-Jurcevic, *Metallomics*, 2020, **12**, 752–757.

74 J. Ma, L. Yan, T. Guo, S. Yang, Y. Liu, Q. Xie, D. Ni and J. Wang, *Sci. Rep.*, 2020, **10**, 10875.
75 J. Baranwal, B. Barse, G. Gatto, G. Broncova and A. Kumar, *Chemosensors*, 2022, **10**, 363.
76 D. Günzel and W. R. Schlue, *BioMetals*, 2002, **15**, 237–249.
77 N. E. L. Saris, E. Mervaala, H. Karppanen, J. A. Khawaja and A. Lewenstam, *Clin. Chim. Acta*, 2000, **294**, 1–26.
78 S. Farahani, D. L. Glasco, M. M. Elhassan, P. Sireesha and J. G. Bell, *Lab Chip*, 2024, **24**, 4096–4104.
79 L. Lvova, C. G. Goncalves, C. Di Natale, A. Legin, D. Kirsanov and R. Paolesse, *Talanta*, 2018, **179**, 430–441.
80 G. Lum, *Lab. Med.*, 2004, **35**, 106–111.
81 H. Frankel, R. Haskell, S. Y. Lee, D. Miller, M. Rotondo and C. W. Schwab, *World J. Surg.*, 1999, **23**, 966–969.
82 V. Chromy, V. Svoboda and I. Stepanova, *Biochem. Med.*, 1973, **7**, 208–217.
83 M. C. Wimmer, J. D. Artiss and B. Zak, *Clin. Chem.*, 1986, **32**, 629–632.
84 C. Kanellopoulou, A. B. George, E. Masutani, J. L. Cannons, J. C. Ravell, T. N. Yamamoto, M. G. Smelkinson, P. Du Jiang, M. Matsuda-Lennikov, J. Reilley, R. Handon, P. H. Lee, J. R. Miller, N. P. Restifo, L. Zheng, P. L. Schwartzberg, M. Young and M. J. Lenardo, *J. Exp. Med.*, 2019, **216**, 1828–1842.
85 M. F. Ryan and H. Barbour, *Ann. Clin. Biochem.*, 1998, **35**, 449–459.
86 W. M. Tsang, M. J. Howell and A. L. Miller, *Ann. Clin. Biochem.*, 1988, **25**, 162–168.
87 T. Fujita, Y. Kawakami, S. Kohda, S. Takata, Y. Sunahara and K. Arisue, *Clin. Chem.*, 1995, **41**, 1302–1305.
88 S. Roudeau, A. Carmona and R. Ortega, *Curr. Opin. Chem. Biol.*, 2023, **76**, 102372.
89 J. Decelle, G. Veronesi, B. Gallet, H. Stryhanyuk, P. Benettoni, M. Schmidt, R. Tucoulou, M. Passarelli, S. Bohic, P. Clode and N. Musat, *Trends Cell Biol.*, 2020, **30**, 173–188.
90 M. C. P. Haigney, B. Silver, E. Tanglao, H. S. Silverman, J. D. Hill, E. Shapiro, G. Gerstenblith and S. P. Schulman, *Circulation*, 1995, **92**, 2190–2197.
91 M. Shechter, T. Saad, A. Shechter, N. Koren-Morag, B. B. Silver and S. Matetzky, *Magnesium Res.*, 2012, **25**, 28–39.
92 N. Zghoul, N. Alam-Eldin, I. T. Mak, B. Silver and W. B. Weglicki, *Diabetes Metab. Syndr. Obes.*, 2018, **11**, 389–400.
93 R. M. L. McFadden, D. Szunyogh, N. Bravo-Frank, A. Chatzichristos, M. H. Dehn, D. Fujimoto, A. Jancso, S. Johannsen, I. Kalomista, V. L. Karner, R. F. Kiefl, F. H. Larsen, J. Lassen, C. D. P. Levy, R. Li, I. McKenzie, H. McPhee, G. D. Morris, M. R. Pearson, S. P. A. Sauer, R. K. O. Sigel, P. W. Thulstrup, W. A. MacFarlane, L. Hemmingsen and M. Stachura, *Angew. Chem., Int. Ed.*, 2022, **61**, e202207137.
94 M. Liu, X. Yu, M. Li, N. Liao, A. Bi, Y. Jiang, S. Liu, Z. Gong and W. Zeng, *RSC Adv.*, 2018, **8**, 12573–12587.
95 W. Hasselbach, *Biochim. Biophys. Acta*, 1957, **25**, 562–574.
96 V. Trapani, G. Farruggia, C. Marraccini, S. Iotti, A. Cittadini and F. I. Wolf, *Analyst*, 2010, **135**, 1855–1866.
97 R. E. London, *Annu. Rev. Physiol.*, 1991, **53**, 241–258.
98 M. S. Afzal, J. P. Pitteloud and D. Buccella, *Chem. Commun.*, 2014, **50**, 11358–11361.
99 A. Loudet and K. Burgess, *Chem. Rev.*, 2007, **107**, 4891–4932.
100 Q. Lin, J. J. Gruskos and D. Buccella, *Org. Biomol. Chem.*, 2016, **14**, 11381–11388.
101 H. M. Kim, C. Jung, B. R. Kim, S. Y. Jung, J. H. Hong, Y. G. Ko, K. J. Lee and B. R. Cho, *Angew. Chem., Int. Ed.*, 2007, **46**, 3460–3463.
102 X. Dong, J. H. Han, C. H. Heo, H. M. Kim, Z. Liu and B. R. Cho, *Anal. Chem.*, 2012, **84**, 8110–8113.
103 H. J. Kim, J. H. Han, M. K. Kim, C. S. Lim, H. M. Kim and B. R. Cho, *Angew. Chem., Int. Ed.*, 2010, **49**, 6786–6789.
104 G. Zhang, J. J. Gruskos, M. S. Afzal and D. Buccella, *Chem. Sci.*, 2015, **6**, 6841–6846.
105 J. J. Gruskos, G. Zhang and D. Buccella, *J. Am. Chem. Soc.*, 2016, **138**, 14639–14649.
106 Y. Matsui, Y. Funato, H. Imamura, H. Miki, S. Mizukami and K. Kikuchi, *Chem. Sci.*, 2017, **8**, 8255–8264.
107 Y. Suzuki, H. Komatsu, T. Ikeda, N. Saito, S. Araki, D. Citterio, H. Hisamoto, Y. Kitamura, T. Kubota, J. Nakagawa, K. Oka and K. Suzuki, *Anal. Chem.*, 2002, **74**, 1423–1428.
108 H. Komatsu, N. Iwasawa, D. Citterio, Y. Suzuki, T. Kubota, K. Tokuno, Y. Kitamura, K. Oka and K. Suzuki, *J. Am. Chem. Soc.*, 2004, **126**, 16353–16360.
109 T. Fujii, Y. Shindo, K. Hotta, D. Citterio, S. Nishiyama, K. Suzuki and K. Oka, *J. Am. Chem. Soc.*, 2014, **136**, 2374–2381.
110 Y. Shindo, T. Fujii, H. Komatsu, D. Citterio, K. Hotta, K. Suzuki and K. Oka, *PLoS One*, 2011, **6**, e23684.
111 O. Murata, Y. Shindo, Y. Ikeda, N. Iwasawa, D. Citterio, K. Oka and Y. Hiruta, *Anal. Chem.*, 2020, **92**, 966–974.
112 H. M. Kim, P. R. Yang, M. S. Seo, J. S. Yi, J. H. Hong, S. J. Jeon, Y. G. Ko, K. J. Lee and B. R. Cho, *J. Org. Chem.*, 2007, **72**, 2088–2096.
113 Q. Lin and D. Buccella, *J. Mater. Chem. B*, 2018, **6**, 7247–7256.
114 I. Alfonso and R. Quesada, *Chem. Sci.*, 2013, **4**, 3009–3019.
115 F. Wu, H. Tong, Z. Li, W. Lei, L. Liu, W. Y. Wong, W. K. Wong and X. Zhu, *Dalton Trans.*, 2014, **43**, 12463–12466.
116 K. Soroka, R. S. Vithanage, D. A. Phillips, B. Walker and P. K. Dasgupta, *Anal. Chem.*, 1987, **59**, 629–636.
117 L. Prodi, F. Bolletta, M. Montalti, N. Zaccheroni, P. B. Savage, J. S. Bradshaw and R. M. Izatt, *Tetrahedron Lett.*, 1998, **39**, 5451–5454.
118 G. Farruggia, S. Iotti, L. Prodi, M. Montalti, N. Zaccheroni, P. B. Savage, V. Trapani, P. Sale and F. I. Wolf, *J. Am. Chem. Soc.*, 2006, **128**, 344–350.
119 G. Farruggia, S. Iotti, L. Prodi, N. Zaccheroni, M. Montalti, P. B. Savage, G. Andreani, V. Trapani and F. I. Wolf, *J. Fluoresc.*, 2009, **19**, 11–19.

120 C. Marraccini, G. Farruggia, M. Lombardo, L. Prodi, M. Sgarzi, V. Trapani, C. Trombini, F. I. Wolf, N. Zaccheroni and S. Iotti, *Chem. Sci.*, 2012, **3**, 727–734.
121 A. Sargenti, G. Farruggia, N. Zaccheroni, C. Marraccini, M. Sgarzi, C. Cappadone, E. Malucelli, A. Procopio, L. Prodi, M. Lombardo and S. Iotti, *Nat. Protoc.*, 2017, **12**, 461–471.
122 N. Kumari, S. Singh, M. Baral and B. K. Kanungo, *J. Fluoresc.*, 2023, **33**, 859–893.
123 J. Orrego-Hernández, N. Nuñez-Dallos and J. Portilla, *Talanta*, 2016, **152**, 432–437.
124 N. Yadav, R. Kumar, A. K. Singh, S. Mohiyuddin and P. Gopinath, *Spectrochim. Acta, Part A*, 2020, **235**, 118290.
125 D. Singh, S. Tomar, S. Singh, G. Chaudhary, A. P. Singh and R. Gupta, *J. Photochem. Photobiol., A*, 2023, **435**, 114334.
126 S. C. Schwartz, B. Pinto-Pacheco, J. P. Pitteloud and D. Buccella, *Inorg. Chem.*, 2014, **53**, 3204–3209.
127 Y. Matsui, K. K. Sadhu, S. Mizukami and K. Kikuchi, *Chem. Commun.*, 2017, **53**, 10644–10647.
128 Y. Matsui, T. Kowada, Y. Ding, P. R. Sahoo, K. Kikuchi and S. Mizukami, *Chem. Commun.*, 2023, **59**, 7048–7051.
129 D. W. Killilea and A. N. Killilea, *Free Radicals Biol. Med.*, 2022, **182**, 182–191.
130 K. P. A. R. Unniram Parambil, A. Silswal, A. Pramanik and A. L. Koner, *Analyst*, 2023, **148**, 2425–2437.
131 A. Silswal, P. Kavyashree and A. L. Koner, *ACS Omega*, 2024, **9**, 13494–13508.
132 M. Brady, V. I. Shchepetkina, I. González-Recio, M. L. Martínez-Chantar and D. Buccella, *J. Am. Chem. Soc.*, 2023, **145**, 21841–21850.